Origins of high $\delta^{18}O$ in 3.7-3.6 Ga crust: a zircon and garnet record in Isua clastic metasedimentary rocks

Laure Gauthiez-Putallaz[1], Allen Nutman[2], Vickie Bennett[1], Daniela Rubatto[1,3]

[1]. Research School of Earth Sciences, Australian National University, Canberra, 2601 ACT Australia

[2]. School of Earth, Atmospheric and Life Sciences, University of Wollongong, NSW 2522, Australia

[3]. Institute of Geological Sciences, University of Bern, CH-3012, Switzerland

Abstract

Elevated $\delta^{18}O$ is used as a marker for the presence of continents and surficial alteration in the Eoarchean and Hadean. This study establishes a timeline for $\delta^{18}O$ enrichment in Eoarchean metasedimentary rocks of the Isua supracrustal belt in Greenland. The source-rocks for the protolith of these metasedimentary rocks are mafic to intermediate magmatic rocks of ≥ 3709 ± 4 Ma, based on the age of zircons found in volcanogenic layers. The $\delta^{18}O$ of +5.4 ±0.4‰ of the zircon crystals indicate that the sources had a primary mantle-derived signature. However, garnet in two metasediments yield higher $\delta^{18}O$ values of + 8.7 to + 9.7 ‰, in equilibrium with a whole-rock of +11 to +12 ‰ at 400-600°C. This requires that the mafic protolith was weathered at surficial conditions, in agreement with previous conclusions based on major element geochemistry. The garnet grains with high $\delta^{18}O$ record four growth zones, assigned to I) arc-building thermal metamorphism, II-III) terrane assembly at medium to high-pressure conditions, estimated to occur at 3660-3690 Ma and IV) late-Archaean overprint likely at ca. 2690 Ma. This shows that material with originally mantle-like $\delta^{18}O$ was altered at low temperature (near-surface) to generate elevated oxygen isotope signatures and then recycled to middle-crustal conditions within 10-50 million years of crystallization in the Eoarchean. We propose that melting of such rocks could produce the zircon crystals with high $\delta^{18}O$ that are found in the detrital and magmatic record in the Archean.

Keywords: Eoarchean, Weathering, Oxygen Isotopes, SHRIMP, Isua, Metasediments

Introduction

The emergence of continents and their interactions with the ocean and atmosphere in the early Earth is key to understanding early life and plate tectonics. Geochemical signatures of relict Eoarchean minerals and rocks offer precious clues about these early events. Among them, oxygen isotopes have been used as a tracer for surficial processes, as the strongest oxygen isotope fractionation occurs by fluid-rock interaction at low temperature (e.g. Lawrence and Taylor, 1971; Gregory and Taylor, 1981). Notably, the discovery of high $\delta^{18}O > 6‰$ in Hadean zircons yielded the first evidence for early crust formation involving a hydrosphere (e.g. Wilde et al, 2001; Mojzsis et al., 2001; Trail et al., 2007). This study focuses on novel evidence for Eoarchaean weathering processes in the Isua supracrustal belt at ca. 3700 Ma, creating heavy oxygen isotope signatures in the protoliths of metasedimentary rocks prior to metamorphism in the Eoarchean.

In order to track protolith signatures and reconstruct multiple stages in the evolution of ancient rocks it is necessary to investigate robust and refractive minerals. In this study, *in situ* measurement of oxygen isotopes by ion microprobe (SHRIMP) in magmatic zircon and garnet is used to track how the $\delta^{18}O$ signature changed from the source to the sediment and throughout metamorphism. Garnet in particular has the capacity to record multiple stages of metamorphism during crustal thickening and collision. Such complex garnet zoning has been described in metasedimentary rocks from the Isua supracrustal belt (Rollinson 2002; 2003) that record a multi-phased metamorphic history, starting potentially as early as 3700 Ma (Blichert-Toft and Frei 2001). Like zircon, garnet can retain primary oxygen isotope signatures up to high temperatures (e.g. Vielzeuf et al. 2005, Higashino et al. 2019). Similarly to previous studies of this type in Phanerozoic metamorphic terranes (e.g. Martin et al. 2014; Page et al. 2014; Rubatto and Angiboust 2015), petrography and garnet chemistry are used to link $\delta^{18}O$ signatures to tectonic events. The inferred protolith signatures are compared to other regional values in order to investigate the degree of surface alteration in Eoarchean sedimentation processes. The $\delta^{18}O$ data are used to establish if any important fluid circulation or metasomatism affected these rocks during metamorphism. Finally, we examine the consequences for the recycling of surficial signatures in the early Earth's crust.

1.1 Geologic context

Owing to the exceptional preservation of a variety of surficial lithologies and of their contact relationships, the Isua supracrustal belt (Figure 1) is unique for the study of the early Earth. Following half a century of research, it has been subdivided into multiple tectonic, geochemical and metamorphic packages (e.g. Nutman et al., 1997; Rollinson, 2002; Nutman and Friend, 2009; Figure 1), which are considered to represent different structural levels of two proto-arcs formed at about 3700 Ma and 3800 Ma (e.g. Nutman et al., 2015a). In this study, we focus on a unit known as the B2 unit (Nutman et al., 1984) of predominantly mafic and lesser felsic metasedimentary schists from the NE part of the Isua supracrustal belt which is part of the 3700 Ma package of Nutman and Friend (2009; Inner Arc Group on Figure 1a), *northwestern tectonic package* of Appel et al. (1998) and *domain II* of Rollinson (2002, 2003). This sedimentary assemblage has been interpreted by Nutman et al. (2015a; 2017) as an arc-related volcano-sedimentary package, consisting of the distal facies of turbidites, derived from andesitic material (Rosing 1999; Bolhar et al. 2004; Bolhar et al. 2005) and deposited into mafic-derived mudstones. The age of the sedimentary protolith is ca. 3705 Ma from sparse zircon dates obtained from four samples (Nutman et al. 1997, 2009; Kamber et al. 2005).

Recent whole-rock studies by Nutman et al. (2015b, 2017, 2019), report high-$\delta^{18}O$ lithologies that are interpreted as the result of Eoarchean low-temperature alteration in the Isua supracrustal belt. High-$\delta^{18}O$ metasedimentary rocks were discovered in the ca. 3700 Ma package. In particular, in the *Central tectonic domain* were identified potential weathered surfaces of andesitic compositions with values of ca. +16 ‰, as well as other metasedimentary rocks, including the B2 schists (values of ca. 12 ‰, Nutman et al. 2017). Significantly, felsic schists from the ca. 3800 Ma domain were reported to contain mantle-signature zircons of magmatic origin and WR $\delta^{18}O$ of 14.6 to 16.2‰ (Nutman et al. 2015a, Hiess et al. 2009), and interpreted as felsic volcanic rocks altered at low-temperature. This study aims at assessing when the B2 schists acquired their high-^{18}O signature and how it evolved during Eoarchean higher-pressure metamorphism.

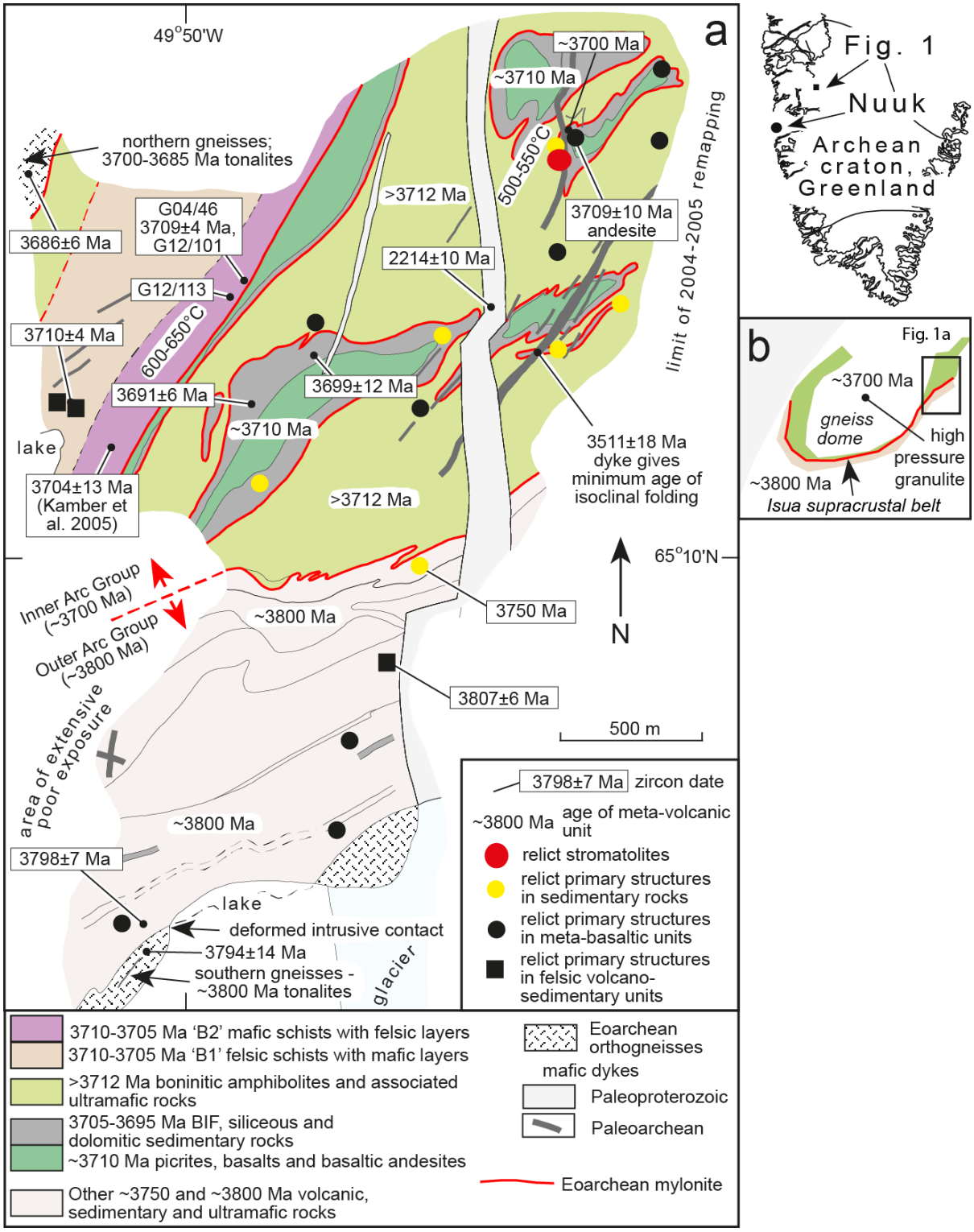

Figure 1. Tectonic map of the eastern part of the Isua Supracrustal Belt (modified from Nutman and Friend, 2009), with previously obtained zircon ages. ***(1,5 columns)***

Previous detailed studies have shown that the Isua metasedimentary rocks have a multi-phased metamorphic history, starting potentially as early as 3700 Ma (Blichert-Toft and Frei 2001). Staurolite and kyanite-bearing assemblages were first recognized by Boak and Dymek

93 (1982), and they indicate a Barrovian-style event at about 600-650°C and 6 kbar. This event
94 was also recognized by Rollinson (2002; 2003) as a Ca-rich annulus present in garnets from
95 the B2 unit. This metamorphic event is unique to the 3700 Ma package Domain II of
96 Rollinson (2002, 2003), and is not recognised in the ~3800 Ma Outer Arc Group package
97 (Fig. 1a) of the Isua supracrustal belt.

98 The B2 unit was intruded by the ~3500 Ma Ameralik dykes a suite of dolerites and norites
99 (McGregor, 1973; Nutman et al., 2004; Fig. 1b). Throughout the Isua area, the Ameralik
100 dykes are weakly deformed to undeformed, and display epidote-amphibolite facies
101 metamorphic assemblages (e.g., Nutman, 1986; Rollinson, 2002). This uniform regional
102 epidote-amphibolite facies metamorphism predates undeformed mafic dykes intruded at
103 2214±10 Ma (Nutman et al., 1995; Fig. 1), and probably occurred in the Neoarchean at ~2690
104 Ma (Nutman and Collerson, 1991). The Ameralik dykes have metamorphic assemblages that
105 indicating uniform Neoarchean P-T conditions and cut tectonic panels of Eoarchean rocks
106 with *different* metamorphic histories (e.g., Rollinson, 2003). This association demonstrates a
107 complex pattern of Eoarchean, pre-3500 Ma metamorphism in the Isua supracrustal rocks.

108 Structurally deeper than the B2 schists, in the refolded gneiss dome north of the Isua
109 supracrustal belt (Fig. 1b), there are rare relicts of 3658±3 Ma, >700°C high pressure
110 granulite assemblages (grt+cpx+pl+qz+hbl+ttn, mineral abbreviations are from Whitney and
111 Evans, 2010) in mafic rocks, which are interpreted, together with the Barrovian-style
112 metamorphism in the B2 schists, as the result of an episode of crustal thickening (Nutman et
113 al., 2013). The high pressure granulite assemblages are in enclaves overprinted by
114 voluminous sheets of 3650-3630 crustally-derived anatectic granites and pegmatites which
115 were emplaced in an extensional regime (Nutman and Bridgwater, 1986; Nutman et al., 2000;
116 Crowley and Myers, 2002). To the south and east of the B2 unit, peak metamorphic
117 conditions are lowest, with maximum temperature of 500-550°C (Fig. 1a; Rollinson, 2003).
118 The domains with the high pressure granulite facies relicts, B2 unit with Barrovian
119 assemblages and the lowest metamorphic grade rocks to the southeast are now horizontally
120 ≤10 km apart, and are partitioned by pre-Ameralik dyke shear zones (Eoarchean mylonites,
121 Fig. 1a). These domains units are interpreted as the centre and margins respectively of an
122 Eoarchean core complex, developed during recovery and extension in the previously
123 thickened crust (Nutman et al., 2013). 3660-3650 Ma anatectic granite sheets are present in
124 both the 3700 Ma Inner Arc group and the 3800 Ma Outer Arc group, which give a minimum

125 age constraint for the crustal thickening event that intervened early in the assembly of the two
126 groups (Crowley, 2003; Nutman et al. 2014). The B2 schists thus represent a rare record of
127 the early metamorphic history of the Isua Supracrustal belt, starting from Barrovian-style
128 crustal thickening event pre-3650 Ma.

129 2 Methods

130 Whole rock (WR) powders were obtained by agate mill grinding. Major elements were
131 measured on fused discs at Geoscience Australia (GA). Fused discs were produced using an
132 Initiative Scientific Products Fusilux 4X4 Fusion Machine using a proportion of 6.000 g of
133 flux for 1.000 g of sample, fusing at 1100°C for 10 min in platinum crucibles. X-ray flux
134 12:22 (35.3% $Li_2B_4O_7$ - tetraborate, 64.7% $LiBO_2$ – metaborate) was used. The flux is
135 certified containing 0-1 ppm of Pb, Ni, Mn, Cd, Zn, Co, Ag; 1-5 ppm K, Cu, Se, As, Al, Sn,
136 Na, Fe; 2-10 ppm Si, S, Ca and Mg. Powder aliquots were measured on a C/H/moisture
137 analyser Leco RC-612 at GA. Fused discs were recovered from XRF analysis, mounted in
138 epoxy disks, cut in their centre and polished. Whole rock (WR) trace elements were measured
139 the Research School of Earth Sciences (RSES) at the Australian National University (ANU)
140 using an ArF excimer laser coupled to a quadrupole Inductively Coupled Plasma Mass
141 Spectrometer (ICP-MS) Agilent 7700. The laser was tuned to a frequency of 5 Hz and energy
142 of 50 mJ (corresponding to a HV of around 26-27kV). The spot size was set to 103 μm.
143 Background was measured for 20 s before 45 s analysis. Calcium, previously determined by
144 XRF, was used as an internal standard. The reported values are the average of 3 spots in the
145 same glass disk. NIST 610 and 612 were used for high (>100 ppm) and low-concentration
146 elements respectively and the BCR basalt (USGS) was used as a secondary standard.
147 Reproducibility and accuracy as assessed on the BCR-2G glass were within 10% or less for
148 all analysed elements. XRF and LA-ICP-MS concentrations were within ±10% of each other
149 for elements V, Zn, Rb, and Zr. The data were reduced with the software Iolite (Paton et al.
150 2001) using the data-reduction scheme for trace elements (Woodhead et al. 2007), followed
151 by an additional step of standardising to the Ca content of the samples.

152 Back-scattered electron (BSE) and secondary electron (SE) investigation of garnet in thin
153 section, as well as Cathodoluminescence (CL) of zircon, were carried out on a JEOL JSM-
154 6610A scanning electron microscope (SEM) at the RSES. Operating conditions for the SEM
155 were 15 kV, a load current of 65–75 μ A and a 10–12 mm working distance. Spot qualitative

major element analyses were obtained with a solidstate Energy Dispersive (EDS) detector on the same JEOL instrument, using an acceleration voltage of 15 kV and a current of 60-70 nA. Analyses were checked for stoichiometry; analyses of UWG2 garnet were within 5% of EMPA analyses on the same UWG2 batch and published values (Valley et al. 1995). X-ray compositional maps were acquired by electron probe micro-analyser (EPMA) in wavelength-dispersive mode. EPMA analyses were carried out with a JEOL JXA-8200 superprobe at the Institute of Geological Sciences (University of Bern). Compositional maps were acquired following the procedure described in Lanari et al. (2012; 2013) using 15 kV accelerating voltage, 100 nA beam current and dwell times of 200 ms. The element maps were acquired with a step size of 6 μm. The compositional maps were classified and converted into maps of garnet endmembers on a 12 oxygen basis using the software XMapTools 2.3.1 (Lanari et al., 2014).

Zircon and garnet trace elements were measured by Laser Ablation ICP-MS at RSES at the conditions described above for WR. Spot sizes of 22 and 28 μm for zircon and of 62 μm for garnet were used. Data were acquired over a 65 seconds analysis that included a 20 s background. Analyses were standardised to NIST 610 (zircon) and NIST 612 (garnet) glasses. Values of Spandler et al. (2011) have been used for data reduction. Stoichiometric Si was employed as internal standard for zircon (SiO_2: 31.6 wt%) and garnet (SiO_2: 42 wt%). Reproducibility and accuracy as assessed on the BCR-2G glass were within ±10% or less for all analysed elements. The data were reduced with the software Iolite (Paton et al. 2011) and its data-reduction scheme for trace elements (Woodhead et al. 2007).

Zircon oxygen isotopes were analysed on the same mounts as used for U-Pb dating with the SHRIMP II instrument at ANU, after a short re-polish and subsequent re-coating, following the analytical procedure described in Ickert et al. (2008). All $\delta^{18}O$ values are reported relative to Vienna Standard Mean Oceanic Water – VSMOW. The standard Temora2 ($\delta^{18}O$=8.2‰, Black et al. 2004, Avila et al. 2019) was used. The repeatability of Temora2 zircon was within 0.5‰ (2σ) during each analytical session. Garnet oxygen isotopes were measured on SHRIMP II and SHRIMP SI at ANU following the method of Martin et al. (2014), and correcting for instrument mass fractionation and compositional bias. The value of the standard garnet UWG2 (5.8 ‰, Valley et al. 1995) was reproduced within 0.3‰ (2σ) in each analytical session. Analyses of garnet and zircon consisted of 5 scans of 20 s for a total counting time of 100 s. Raw data were processed with the in-house software POXI-MC. For

garnet, a matrix correction for grossular content was made according to calibrations by Martin et al. (2014) acquired in the same year as the unknown analyses, with similar tuning and running parameters. Garnet chemistry was acquired by EDS analysis, measured *a posteriori* next to each SHRIMP spot. Error propagation for oxygen isotope analyses follows Martin et al. (2014).

Zircon U-Pb dating was performed on the SHRIMP II at ANU, using a setup modified from Williams (1998). Standards and unknowns were analysed with a spot size of around 20 by 25 µm. Temora2 zircon (U-Pb age of 417 ± 1 Ma, Black et al. 2003) was used as standard for instrumental U-Pb mass fractionation and U concentration (160 ppm). The calibration error during the analytical sessions was 1.5% and this uncertainty was propagated in quadrature to individual analyses. Ratios were corrected for common Pb according to the measured $^{204}Pb/^{206}Pb$ ($^{4/6}R_m$) and the non-radiogenic $^{204}Pb/^{206}Pb$ ($^{4/6}R_c$) following the method described in Williams (1998), i.e $f_{206} = {}^{4/6}R_m / {}^{4/6}R_c$. The $^{4/6}R_c$ composition was assumed to be that predicted by Stacey and Kramers (1975) model. Most analyses yield less than 1% common ^{206}Pb, so the choice of the common Pb model has no significant impact on the ages. Data reduction and assessment was performed using MS Excel extensions SQUID 2.5 (Ludwig 2009) and Isoplot 4 (Ludwig 2012).

3 Results

3.1 Sample petrography

The B2 unit (Nutman et al. 1984, 1997), outcrops as an extensive sequence of layered biotite-chlorite-garnet schists over ca. 5 km along strike. Most layers are coarse-grained with cm-sized garnets embedded in a matrix of chlorite with quartz layers, and quartz and calcite veinlets. Many layers contain pale-blue pseudomorphs made of finely grained white mica interspersed with staurolite relicts and chloritoid. Kyanite was found in samples of the same unit by Boak and Dymek (1982) but was not observed in this study. Two mafic schist samples (G12/101, G12/113) were studied in detail for thin section petrography and garnet zoning (Table 1). Zircon grains from a more felsic sample (G04/46) were used for U-Pb dating and oxygen isotope analysis.

216

217 **Table 1. Sample characteristics. Mineral abbreviations are from Whitney and Evans *(2010)*.**

Sample #	Rocktype	Area	Latitude	Longitude	Mineralogy	Facies
G12/101	chlorite-garnet schist	Isua	65°10'26.5"	49°49'40.2"	Chl, Grt, Qz, Ms, Pl, Tur, Ilm, Cal	Amphibolite
G12/113	garnet-chlorite fels	Isua	65°10'18.6"	49°49'58.6"	Chl, Grt, Qz, Ms, St, Cld, Tur, Ilm	Amphibolite
G04/46	plagioclase-amphibole gneiss	Isua	65°10'26.5"	49°49'40.2"	Qz, Pl, Bt, Chl, Grt, Ilm, Zrn	Amphibolite

218

219 G12/101 is a fine layered plagioclase-chlorite-garnet-quartz-tourmaline schist with 5-10 mm
220 garnet crystals (Figure 2); G12/113 is a more quartz-rich garnet-chlorite rock with minor
221 tourmaline and numerous staurolite relicts and pseudomorphs after staurolite (Figure 2,
222 Figure 3a). Some of these staurolite pseudomorphs contain chloritoid needles that grew over
223 staurolite relicts, statically over the main foliation. In both samples, garnet shows rotational
224 structures compared to the main foliation (Figure 3b).

225 G04-46 is a layered felsic gneiss in which biotite and chlorite-rich layers contain more garnet
226 than quartz-rich layers. In quartz-rich layers, garnet grows in a skeletal texture, which
227 impedes the interpretation of outwards growth zoning. Small (ca. 200 μm) garnet crystals in
228 the chlorite-rich layers yield concentric zoning that is similar to what is observed in the
229 chlorite schists G12-113 and G12-101 (Figure 2c, d).

230

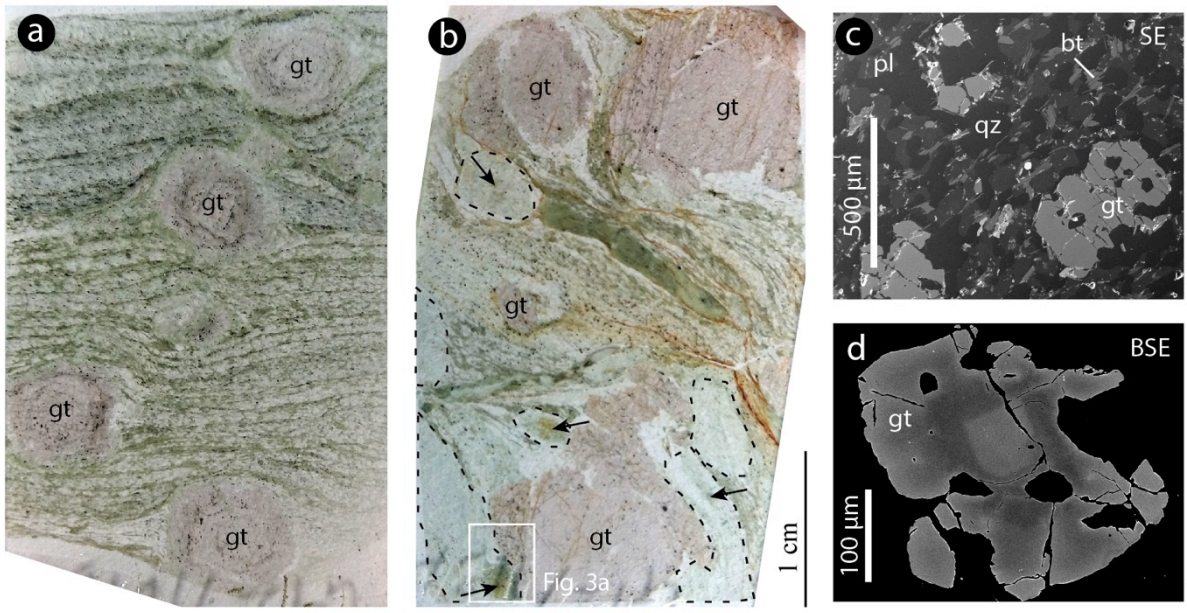

Figure 2. Thin-section optical scan showing the microtexture of samples G12/101 (*a*) and G12/113 (*b*). In G12/113, the dotted lines outline staurolite pseudomorphs and the arrows indicate staurolite relicts. (*c)* Secondary-electron image of a quartz-rich layer showing the mineral distribution. (*d) BSE* image of a garnet grain in sample G04/46 showing chemical zoning. *(2 columns)*

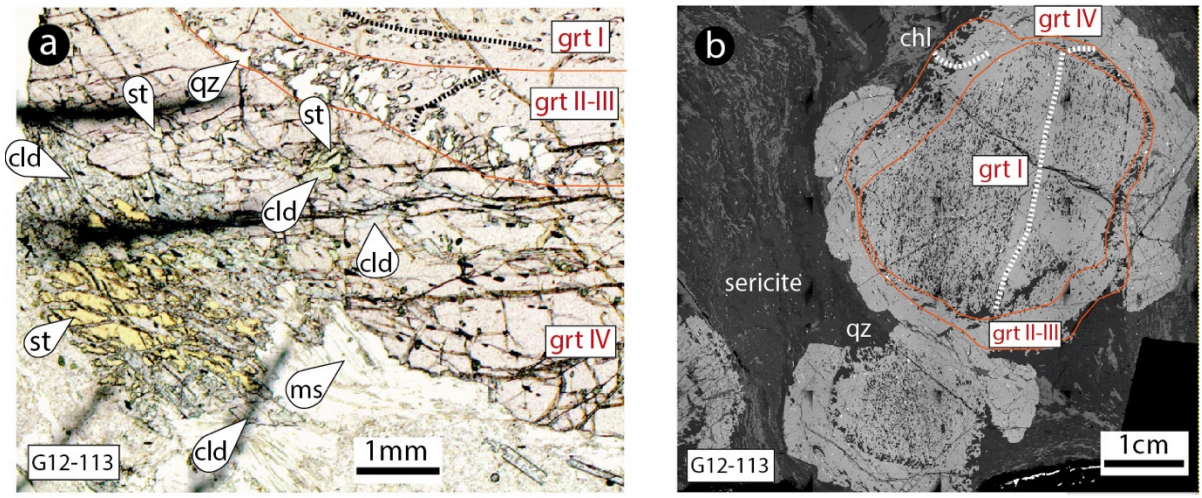

Figure 3. (*a)* G12/113 transmitted light photomicrograph of matrix and garnet inclusion mineralogy: Garnet Zone IV (grt IV) contains inclusion of relict staurolite and of chloritoid. Garnet Zones I to IV correspond to chemical zones described in text. (*b)* G12/113 Back-scattered-electron image of two garnet grains showing the rotation of inclusion trails (dotted lines) and the textural relationship between zones (red lines). *(2 columns)*

3.2 Whole Rock Geochemistry

Sample G12/101 and G12/113 are mafic to intermediate in composition (51.7 and 60.9 wt% SiO_2, Table 2), they are both rich in Al_2O_3 and Fe_2O_3, but G12/113 is much poorer in alkalis than G12/101. Gneiss G04/46, from which the zircon crystals were separated, is more felsic with 75.6 wt% SiO_2.

Mafic schists G12/101 and G12/113 have parallel trace element patterns that are enriched in incompatible elements compared to the primitive mantle (Figure 4a). Both samples have a marked negative Nb-Ta anomaly, a positive Zr-Hf anomaly and slight positive Eu and Sr anomalies.

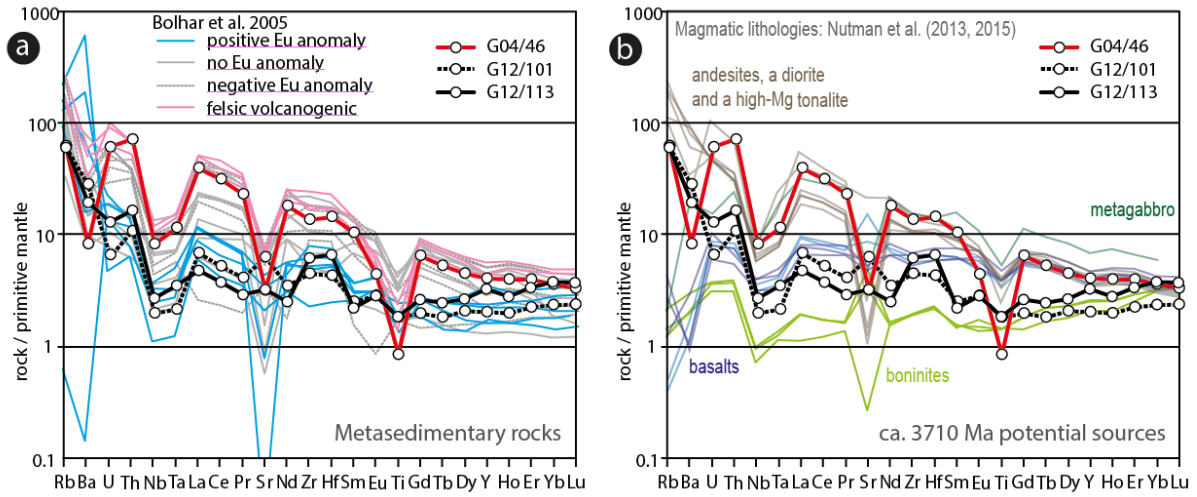

Figure 4. Trace element patterns of investigated samples normalised to primitive mantle from Sun and McDonough (1989) compared to literature data. (*a) Comparison with* sedimentary lithologies from Isua (Bolhar et al. 2005). (*b) Comparison with* the ca. 3710 Ma magmatic lithologies (Nutman et al. 2013, 2015). *(2 columns)*

Felsic layer G04/46 is enriched in incompatible elements (Figure 4b) but with marked negative anomalies in Ba, Nb-Ta, Sr, Eu and Ti. The anomalies imply the fractionation of plagioclase and a Ti phase, which is also typical of other Isua dioritic and tonalite rocks of equivalent age (e.g. Nutman et al., 2013).

Aliquots of the G04/46, G12/101 and G12/113 whole-rock powders were analysed for $\delta^{18}O$ using the conventional fluorination technique (data reported in Nutman et al., 2017, method described in Nutman et al, 2015a) and yielded values between +11.8 and +13.0‰, with an

265 analytical uncertainty is 0.1 ‰ (1σ). Repeated analysis of samples G12/101 and G12/113
266 after further hand-crushing yielded slightly lower $\delta^{18}O$ value of +11.5 and +11.6‰,
267 respectively.

268 **Table 2. XRF Major and LA-ICP-MS trace element composition of Isua samples.**

	G04/46	**G12/101**	**G12/113**
XRF (wt%)		**chl-grt-qz-pl-tur**	**chl-grt-qz-st**
SiO_2	75.6	51.7	60.9
Al_2O_3	10.1	20.5	16.0
Fe_2O_3	6.9	13.0	13.4
MnO	0.1	0.2	0.7
MgO	2.6	4.1	2.2
CaO	1.5	2.4	1.1
Na_2O	1.3	3.2	1.7
K_2O	0.7	1.3	1.2
P_2O_5	bdl	bdl	bdl
TiO_2	0.2	0.4	0.4
XRF Sum	**98.9**	**96.7**	**97.6**
H_2O (LECO wt%)	2.0	3.7	2.1
CO_2 (LECO wt%)	0.2	0.7	0.1
Total Sum	**101.3**	**101.3**	**100.0**
Nutman et al. 2017			
$\delta^{18}O_{VSMOW}$ (‰)	**+13.0 (+13.0)**	**+11.6 (+11.8)**	**+11.5 (+12.6)**
LA-ICP-MS (µg/g)			
Sc	12.3	45.4	43.5
Ti	1083	2341	2325
V	29.0	204	138
Cr	76.1	1033	726
Mn	500	1369	4751
Co	14.5	60.0	36.9
Ni	47.3	434	185
Cu	3.5	5.5	41.7
Zn	38.0	96.5	28.9
Ga	14.8	23.4	17.3
Ge	11.0	7.6	13.0
Rb	39.6	39.7	39.7
Sr	66.5	132	66.6
Y	18.3	9.1	14.5
Zr	152	49.9	68.9
Nb	5.9	1.4	1.9
Cs	0.9	0.4	0.4
Ba	57.6	198	137
La	27.2	4.7	3.2
Ce	56.0	9.2	6.5
Pr	6.4	1.1	0.8
Nd	24.6	4.7	3.3
Sm	4.6	1.1	1.0
Eu	0.7	0.5	0.5
Gd	3.8	1.2	1.5
Tb	0.6	0.2	0.3
Dy	3.3	1.5	1.9

Ho	0.6	0.3	0.4
Er	1.9	1.1	1.6
Tm	0.3	0.2	0.3
Yb	1.8	1.1	1.8
Lu	0.2	0.2	0.3
Hf	4.5	1.3	2.0
Ta	0.5	0.1	0.1
W	0.5	1.3	0.6
Pb	7.3	14.5	8.4
Th	6.2	0.9	1.4
U	1.0	0.1	0.3

3.3 Zircon geochronology and geochemistry

Sparse, small prismatic zircon crystals were recovered from sample G04/46. They are mostly oscillatory zoned (Figure 5a), which is a common feature of magmatic zircons (e.g. Hoskin and Schaltegger 2003). The zircon oscillatory-zoned cores display embayments and very narrow (< 10 μm) overgrowths that are bright in CL and that could not be analysed in sectioned crystals because of their small size. It is speculated that the overgrowths indicate a fluid related dissolution-reprecipitation event, probably during metamorphism. Oscillatory-zoned domains in G04/46 zircon crystals yield a weighted mean $^{207}Pb/^{206}Pb$ age of 3709 ±4 Ma (MSWD = 1.2, 11 analyses) and a Concordia age of 3709 ±6 Ma (95% confidence level; Figure 5a,b; *Supplementary material 1*). These domains have Th/U between 0.6 and 1.1, typical of intermediate to mafic igneous zircon (e.g. Hoskin and Schaltegger, 2003). The common Pb content of the analyses is below 1% in all cases.

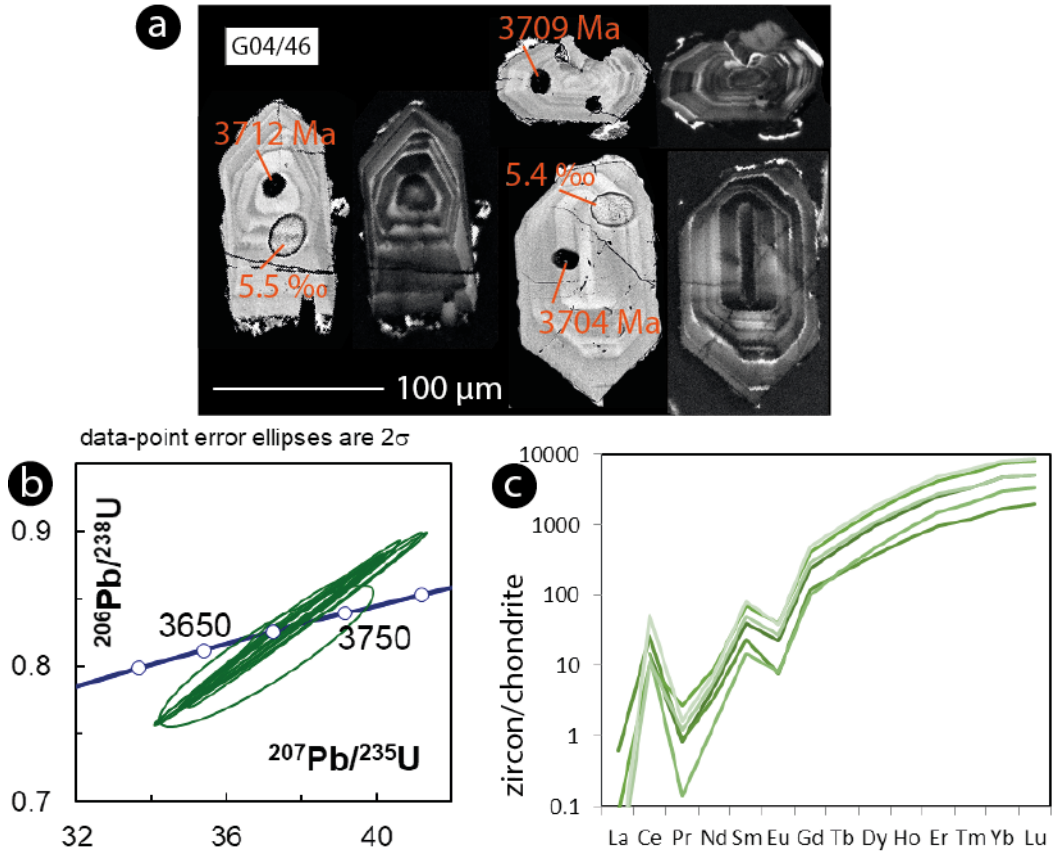

Figure 5. ***a.*** **High-contrast BSE (left) and CL images (right) of selected zircon grains from felsic gneiss G04/46. The 204-corrected ^{206}Pb-^{207}Pb age (in Ma) is reported beside U-Pb dating pits (black). $\delta^{18}O_{VSMOW}$ values (in ‰) are reported beside the shallow SHRIMP pits.** ***b.*** **Wetherill Concordia plot for 204-corrected U-Pb data.** ***c.*** **REE composition of zircon normalised to CI chondrites of Sun and McDonough (1989) different shades of green are used for individual grains.** ***(1,5 columns)***

The REE pattern of the oscillatory zones shows a negative Eu anomaly and a positive Ce anomaly, together with strong HREE enrichment. The patterns are similar to what is documented for Phanerozoic magmatic zircons (e.g. Hoskin and Schaltegger, 2003; Figure 5 c, *Supplementary material 2*). Oxygen isotopes were measured in oscillatory-zoned zircon grains (Figure 6a, *Supplementary material 3*). The results return a homogenous population of typical mantle $\delta^{18}O$ value at +5.4 ±0.4‰ (1sd, n=20). One zircon as inclusion within a garnet was analysed *in situ* and also yields a mantle-like value of +6.0‰ (Figure 6b). One single zircon rim in a fractured grain yields a distinctly higher $\delta^{18}O$ of 10.1 ±0.1‰ (1SE).

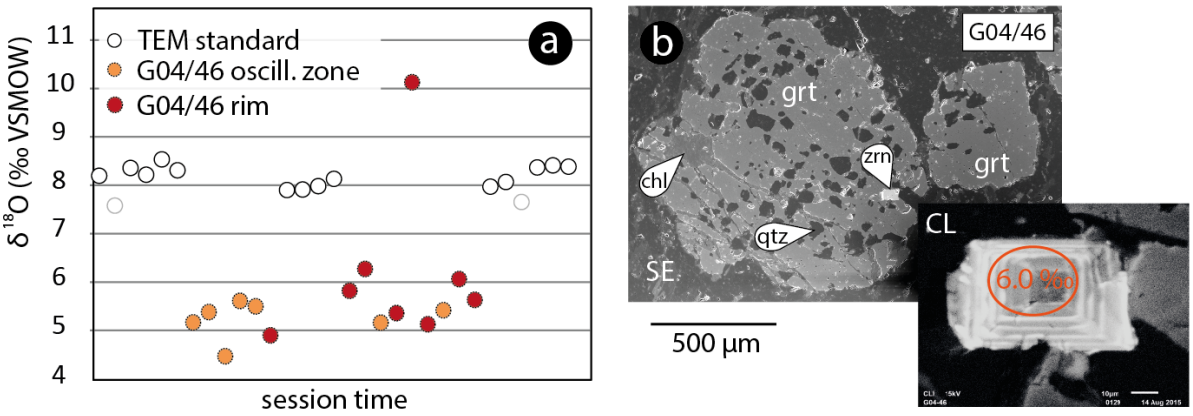

Figure 6. a. SHRIMP oxygen isotope analyses of Isua zircon plotted along session time (arbitrary scale). Internal 1SE bars are smaller than symbols. Shaded symbols are data points that were rejected on the basis of instrument parameters. b. Secondary-electron image of G04/46 garnet with zircon inclusion; the cathodoluminescence images of the zircon is shown in the bottom right with marked the location of the oxygen isotope analysis and the $\delta^{18}O_{VSMOW}$ value. ***(2 columns)***

3.4 Garnet geochemistry

Typical garnet crystals in both samples (8 mm across in sample G12/101 and 15 mm across in G12/113) show a zoning pattern consisting of 4 distinct zones from core to rim that are identified on the basis of texture and major elements (Figure 3b, Figure 7, *Supplementary material 4*, *5*). Generally, Mn decreases (Sps_{0-18}) and Mg increases (Alm_{68-88}) from core to rim, and sharp changes in Ca content mark the zones. Zone I defines the garnet core, and is relatively rich in Mn and poor in Ca (G12/101-*I*: Prp_{4-5}, Grs_{8-9}, Sps_{13-19}, $Alm_{68-73;}$ G12/113-*I*: Prp_{4-5}, Grs_{5-7}, Sps_{9-18}, Alm_{72-81}); the Mn concentration has a slight bell-shaped profile from the inner to the outer part of the core. In sample G12/113, this zone yields numerous quartz inclusions that define an internal foliation (Figure 3b). Zone II is marked by a sharp increase in Ca that then decreases outwards, and a gradual decrease in Mn (G12/101-*II*: Prp_{4-5}, Grs_{15-21}, Sps_{8-14}, $Alm_{64-72;}$ G12/113-*II*: Prp_{4-5}, Grs_{8-11}, Sps_{6-8}, Alm_{79-81}). This zone contains larger inclusions. Zone III is again marked by sharp increase in but with even lower Mn content (G12/101-*III*: Prp_{4-6}, Grs_{19-21}, Sps_{1-5}, $Alm_{71-73;}$ G12/113-*III*: Prp_{4-6}, Grs_{7-16}, Sps_{1-5}, Alm_{77-85}). Zone IV is the outer rim and is characterised by another sharp change in Ca to low concentrations comparable to the core, and by the highest Mg content (G12/101-*IV*: Prp_{6-9}, Grs_{5-12}, Sps_{0-4}, $Alm_{79-85;}$ G12/113-*IV*: Prp_{6-10}, Grs_{3-8}, Sps_{0-1}, Alm_{85-88}).

The sharp boundaries observed between the core and Zone II as well as between Zone II and III in G12/101 (Figure 7a) are underlined by the presence of µm-sized mineral and fluid inclusions. Ilmenite, rutile, plagioclase, quartz, tourmaline and chlorite are inclusions in zone I of garnet G12/113. In zone II, rutile, ilmenite, tourmaline and quartz were found. Zone III yields tourmaline and ilmenite, while rutile can be observed in cracks. Zone IV is generally inclusion-poor, but in one instance, it contains composite inclusions of staurolite and chloritoid (Figure 3a), similar to pseudomorphs observed in the matrix.

In both samples, the garnet core (Zone I) is the most enriched in HREE (Figure 7d, *Supplementary material– 6*), with a gradual depletion towards the outer core similar to what is observed for Mn, a proxy of Rayleigh fractionation during garnet growth. This fractionation trend results in a change in HREE concentrations of two orders of magnitude in sample G12/113 that contains large garnet grains. Zone I yields a marked Eu anomaly in both samples, which is indicative for the presence of plagioclase in the co-existing assemblage because neither of these samples shows negative Eu anomalies in their whole-rock composition (Figure 4). Zone II and zone III display no Eu anomalies in both samples, which suggests that plagioclase reacted out or significantly decreased in abundance during this stage. The HREE content of these garnet zones is generally lower than Zone I, indicating that most HREE were fractionated in the garnet cores. Zone IV yields different REE signatures in the two samples. In sample G12/113, Zone IV yields a small to negligible negative Eu anomaly; this is in line with only minor plagioclase in the matrix, which is and restricted to thin layers (mode ca. 0.5-1%). Particularly in sample G12/113 that contains large garnet grains, Zone II and IV have extreme depletion in M-HREE, which is interpreted as an effect of the fractionation of HREE in the inner garnet zones. In sample G12/101, the garnet rim yields a marked negative Eu anomaly and this is correlated to the presence of plagioclase in the matrix (mode ca. 40%).

G04/46 is a layered felsic rock in which amphibole and chlorite-rich layers contain more garnet than quartz-rich layers. In quartz-rich layers, garnet grows in a skeletal texture that impedes the interpretation of outwards growth zoning. Garnet in the amphibole-rich layers yields concentric zoning that is similar to what is observed in the schists G12/113 and G12/101.

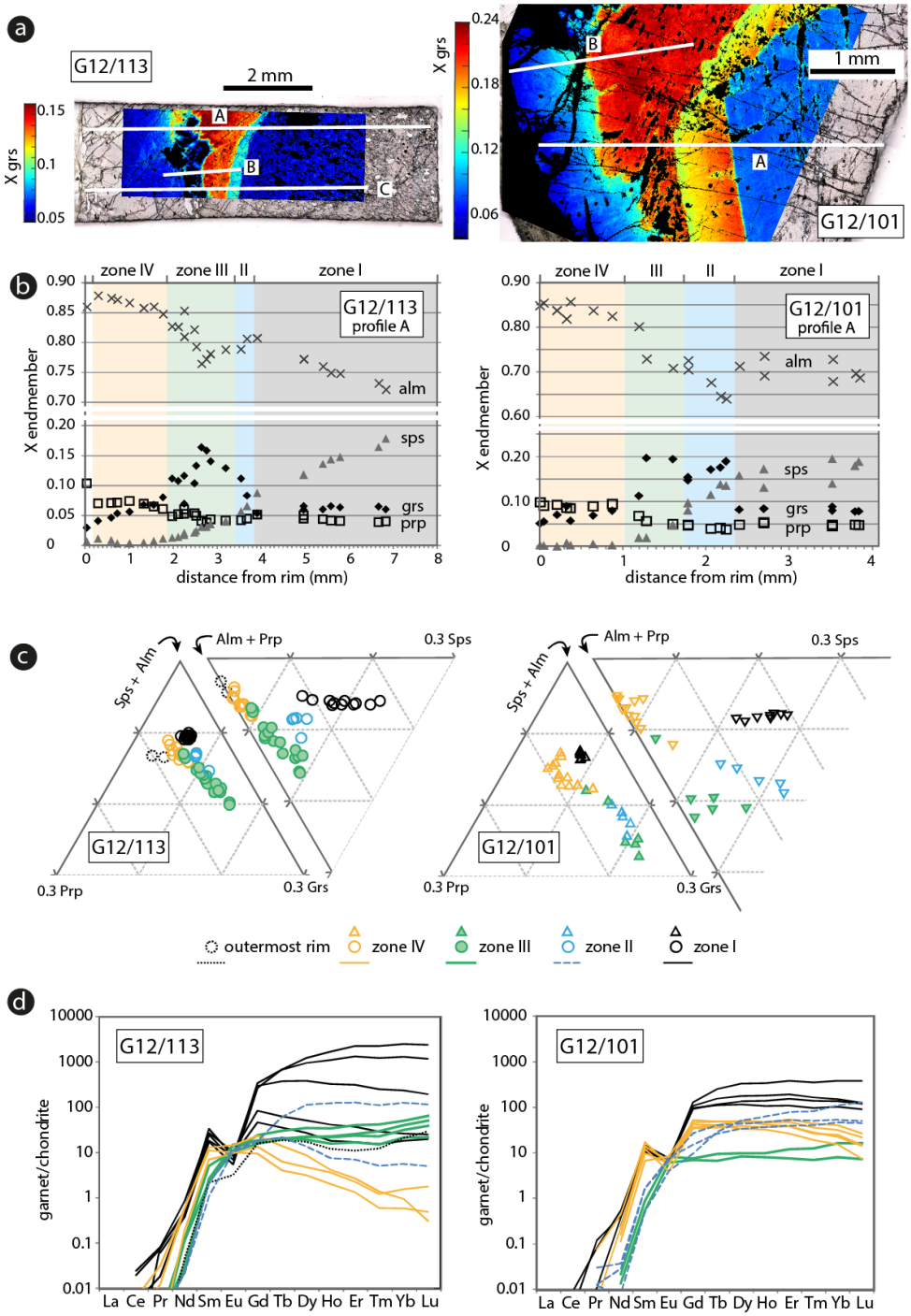

Figure 7. Chemical composition of garnet from B2 schists. a. EMPA garnet maps of XGrs superimposed on the transmitted light photograph of analysed garnet grains; the white lines indicate the location of the compositional profiles. b. EDS endmember composition profiles according to distance to rim (analysis position projected on profile line, zones are distinguished on the basis of texture and chemistry). c. Endmember composition of garnet zones. d. REE composition of different garnet zones normalised to CI chondrites of *Sun & McDonough (1989)*. *(2 columns)*

Oxygen isotope analyses were performed in each zone along two core-rim profiles in garnet G12/113 (length of profile: 7 mm). In addition, a third and more detailed profile of the garnet mantle was measured (Figure 8, *Supplementary material 7*). In garnet G12/113, the core yields an average $\delta^{18}O$ of +9.2 ±0.1 ‰ (1sd, n=11), Zone II +9.7 ±0.3 ‰ (1sd, n=5), zone III +9.4 ±0.2 ‰ (1sd, n=19) and zone IV 8.7±0.3 ‰ (1sd, n=15). The total uncertainty for these averages calculated following the procedure of Martin et al. (2014) is in the range of 0.5-0.6 ‰ (2σ), and is dominated by the grossular and spessartine matrix calibration uncertainty. For consistency, both grossular and spessartine corrections were applied in all measurements, even though the correction for spessartine is negligible for zone III and IV compositions.

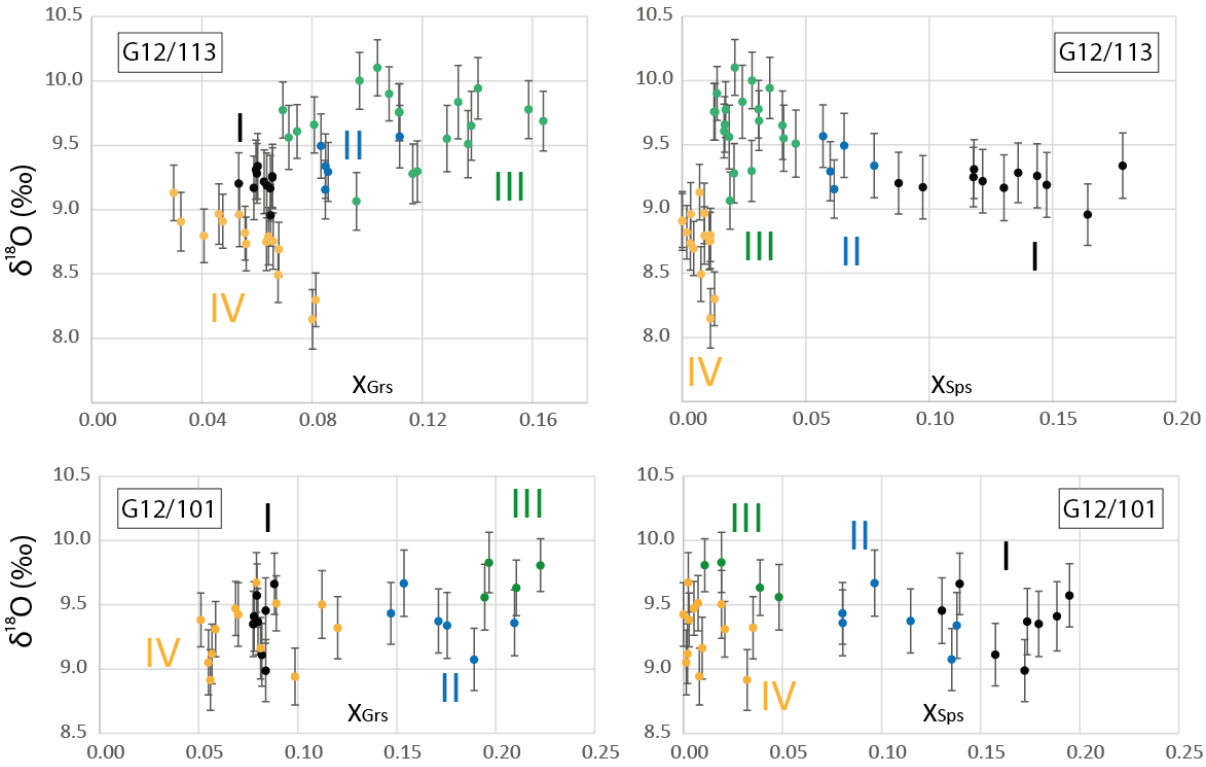

Figure 8. SHRIMP IMF-corrected oxygen isotope analyses from profiles in G12/113 and G12/101 garnet, displayed according to their grossular and spessartine endmember content. Profile positions are indicated on Figure 7. Figure $\delta^{18}O$ values are plotted with 1σ error bars. Symbol colour coding represents the garnet Zone I to IV as identified by texture and major elements in Figure 7. ***(2 columns)***

Similarly, two rim–core profiles were measured in garnet G12/101 (length 4 mm, Figure 8). In this smaller garnet, less variation is observed from core to rim, from a $\delta^{18}O$ of +9.4 ±0.2

(1sd, n=8) in the core (zone I), Zone II +9.4 ±0.2 ‰ (1sd, n=6), zone III +9.7 ±0.1 ‰ (1sd, n=4), to a value of +9.3 ±0.2 (1sd, n=13) in the external rim (IV).

4 Discussion

4.1 Sedimentary source of the Isua B2 schists

From major and trace element data, it has been inferred that the B2 schists are predominantly derived from mafic sources (Dymek et al. 1983; Nutman et al. 1984; Bolhar et al. 2005). The two schists investigated here are comparable in trace element composition to the more mafic rocks in Nutman et al. (2013), more specifically boninites and basalts(Figure 4).The high contents in Cr and Ni in samples G12/101 and G12/113 are in line with a protolith rich in mafic minerals such as olivine, clinopyroxene and spinel. The contribution of mafic sources derived from depleted mantle, such as Isua supracrustal belt ≥3710 Ma boninites and basalts, was specifically proposed by Polat et al. (2002) and Nutman et al. (2015a). The trace element composition of G12/101 and G12/113 have strong similarities to the samples with positive Eu anomalies identified by Bolhar et al. (2005), which the author interpreted as clastic sediments derived from mafic sources, for which the Eu anomaly was developed because of precipitation of marine Fe-oxyhydroxides during deposition or diagenesis.

The trace element pattern of felsic rock G04/46 (Figure 4) is similar to felsic volcanogenic samples in Bolhar et al. (2005) and fresh ca. 3710 Ma andesites (Nutman et al. 2013). The high-SiO_2 content of the felsic layer is not due to later silica veining, because the unit is uniformly fine-grained. Instead it is likely due to silification of a volcanic layer at the surface – a process widespread in Archean volcanic rocks. This modification of the composition is in keeping with (i) the low yield of zircons in this sample (more akin with an andesitic rather than a dacitic or rhyolitic volcanic source) and (ii) the small size of the zircons (≤100 μm), suggesting rapid cooling of the source magma in an eruptive environment.

The zircon grains from this sample yield magmatic CL zoning and REE profiles, as well as mantle-like $\delta^{18}O$ (ca. +5.3 ‰). They yield a concordia age of 3709 ±6 Ma, which is within the range of ages for volcanic rocks in the B2 unit (3700-3710 Ma, Kamber et al. 2003). The distinction between a strictly volcanic and a volcano-sedimentary origin cannot be made due to the lack of preserved structures. The euhedral shape of the zircon crystals, as well as trace

element similarities between G04/46 and fresh andesites suggest that the protolith underwent no or limited sedimentary sorting and transport . This age is interpreted as the eruption age, or the source-rock age for this layer and it in turn constrains the deposition of the surrounding sediments to ca 3710 Ma at the earliest.

4.2 Weathering signatures within the 3700 Ma unit

The Itsaq Gneiss Complex rocks have been previously investigated for their oxygen isotope composition (Figure 9). Oxygen isotopes have been measured in a variety of lithologies, either as whole rock (Baadsgaard et al. 1986; Cates and Mojzsis 2006; Furnes et al. 2007; Pope et al. 2012) or mineral separates (Cates and Mojzsis 2006; Pope et al. 2012), as well as *in situ* in zircon and olivine grains (Cates and Mojzsis 2006; Hiess et al. 2009; Hiess et al. 2011).

The magmatic lithologies inferred to be the source for the B2 sedimentary rocks (boninites, island-arc-tholeiites and andesites, Figure 9), which outcrop in the 3700 Ma package of Isua supracrustal belt, yield mantle-like or slightly higher whole-rock $\delta^{18}O$ values. This signature is also recorded by magmatic zircon in G04/46 that yield mantle-like $\delta^{18}O$ values (+4.5 to +6 ‰). This can be recalculated (e.g. Valley et al., 2003) to a whole-rock value of +7 to +8 ‰ for the protolith magma, similar to the values reported for coeval quartz diorites and tonalities in the Isua supracrustal belt (Figure 9). The $\delta^{18}O$ bulk rock values for sample G12/101, G12/113 and G04/46 (+11.6, +11.5 and +13.0 respectively, as reported in Nutman et al. 2017) are higher than reported values for any fresh, unaltered Isua 3700 Ma magmatic rocks. Low-temperature fluid-rock interaction is thus required to elevate the whole-rock $\delta^{18}O$ value to approximately +12 ‰ in the three samples studied here. The process of Eoarchean weathering has been documented in the Isua supracrustal belt: Nutman et al. (2017, 2019) reported whole-rock $\delta^{18}O$ values of between +15.7 to +16.8 for altered weathered mafic rocks located just below a ~3700 Ma unconformity in the *central tectonic domain*. They provide an analogue for the source-rock of the B2 schists. Other similar high $\delta^{18}O$ values are reported from a few other localities of the Itsaq Gneiss Complex, which is an indication that early, low temperature alteration/weathering might have been widespread. For example this is observed in an extensive felsic schist unit in the 3800 Ma package of the Isua supracrustal belt (Nutman et al. 2015b) as well as Akilia association biotite-quartz-garnet rocks ca. 200 km south of Isua (Cates & Mojzsis, 2006).

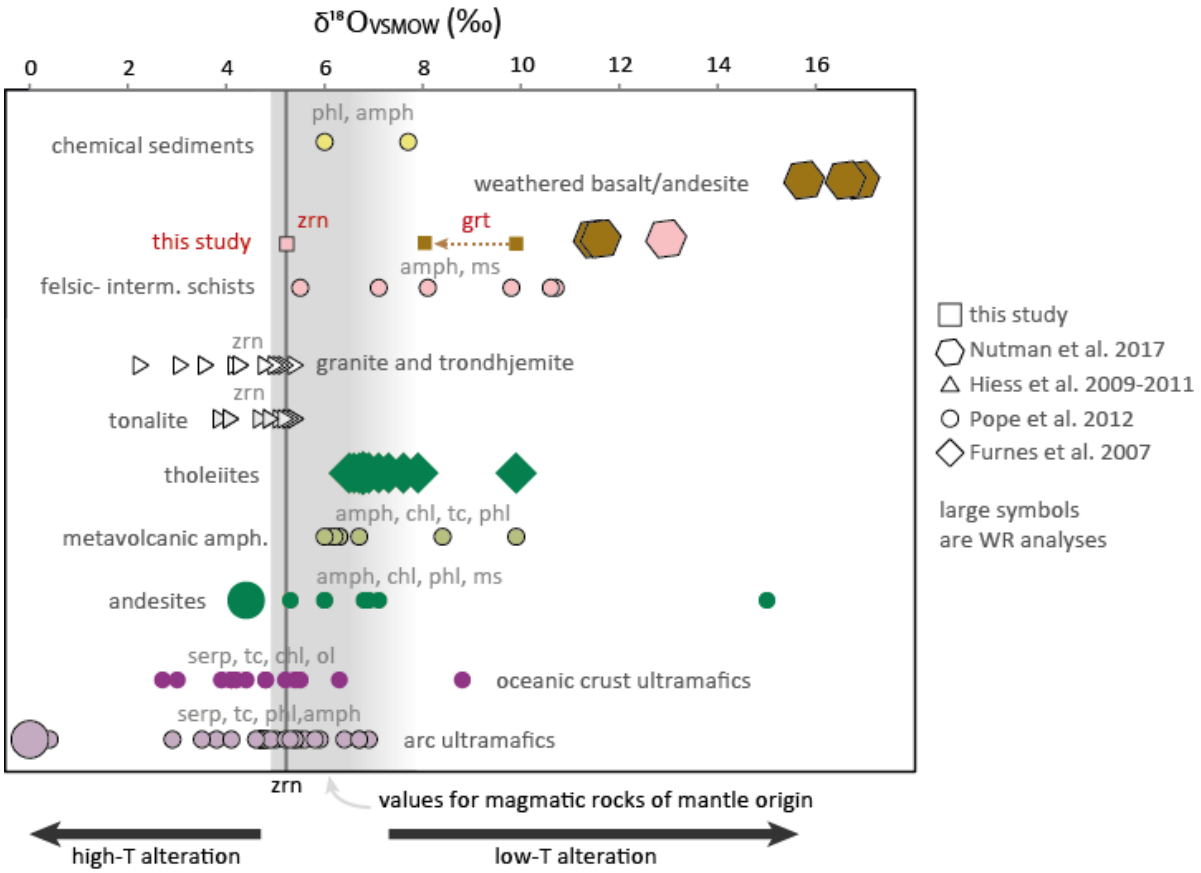

Figure 9. Summary of oxygen isotope data for rocks of the 3700 Ma package of the Isua supracrustal belt, extracted from Hiess et al. (2009), Hiess et al. (2011), Pope et al. (2012), Furnes et al. (2007) and Baadsgaard et al. (1986) according to the geochronology and mapping of Nutman & Friend (2009). Mantle zircon value is taken from Valley et al. (1998), the grey band represents the range of magmatic rocks derived from the mantle, following fractional crystallisation with little alteration. Square symbols represent minerals data acquired from the samples studied in this work; corresponding whole-rock analyses were reported in Nutman et al. (2017) as part of a larger dataset. ***(2 columns)***

Temperatures required to enrich the $\delta^{18}O$ of silicates to this degree are below 200°C (e.g. Sheppard and Gilg, 1996 and references therein). The foremost mechanism by which high $\delta^{18}O$ are achieved on modern Earth is the formation of kaolinite, smectite and other clay minerals in weathering of magmatic/volcanic rocks exposed to the surface (e.g. Savin and Epstein, 1970). This surficial weathering process is supported by major element indicators as shown in Figure 10 in the diagram of Ohata and Arai (2007) based on oxide proportions for Si, Ti, Al, Fe, Mg, Ca, Na and K. This diagram features a mafic-felsic trend where igneous

rocks lie, the grey arrows represent weathering trends from the igneous poles as observed in soil weathering profiles. The major element composition of the mafic schists in the B2 unit forms a trend from the andesite field down to the weathering corner of the diagram corresponding to soils composition, in agreement with previous data on Isua metasedimentary rocks (Nutman et al. 2013, Bolhar et al. 2005). This trend represents leaching of low-temperature fluid-soluble elements, namely by replacement of plagioclases by kaolinite (or similar reactions forming clay minerals; Ohata and Arai, 2007).

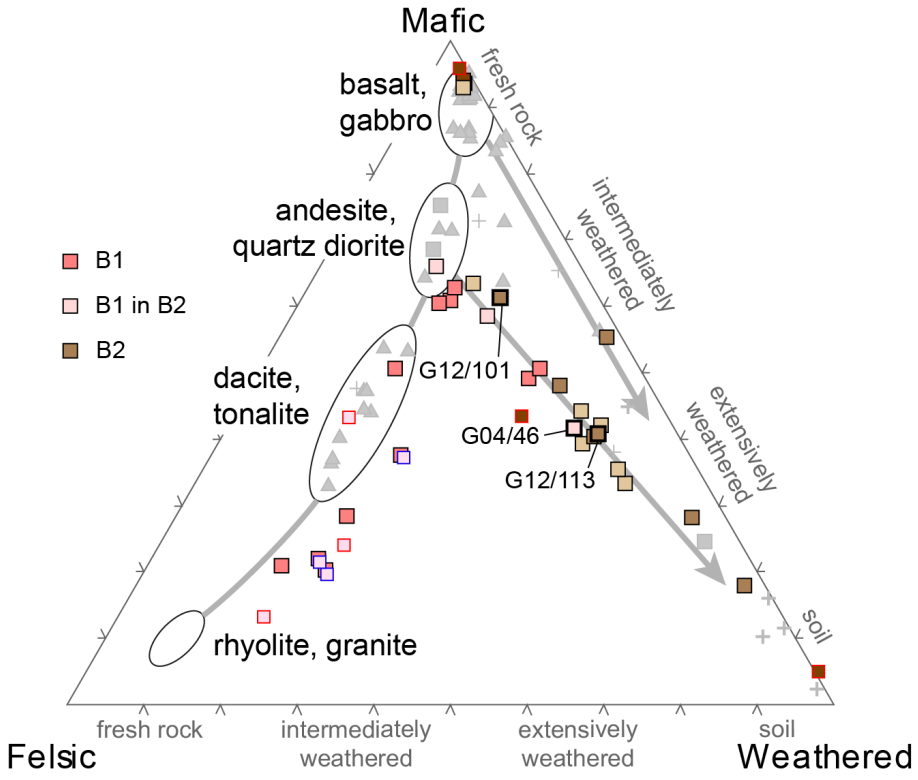

Figure 10. Weathering diagram of Ohata & Arai (2007) for samples G12/101, G12/113 and G04/46 together with B1 felsic schists and B2 mafic schists (pink and brown squares, respectively), with representative ~3700 Ma lithologies (grey symbols, Nutman et al. 2015). B1 and B2 literature data is from Nutman et al. (2013) in the black outlines, Bolhar et al. (2005) in the blue outlines. ***(2 columns)***

4.3 Garnet growth in Isua B2 schists

Because of its large stability field and resistance to chemical re-equilibration, zoned garnet have the potential of recording multiple tectonic events, and with it variable $\delta^{18}O$ signatures. In order to unravel such complex evolution, a first step is identifying growth zones and their relationship to metamorphic/tectonic stages in the Isua supracrustal belt. In B2 samples

G12/113 and G12/101, garnet is chemically zoned, as observed by previous authors in other samples from the same unit (Rollinson, 2002; Rollinson, 2003, and to a lesser extent Boak & Dymek, 1982). These garnet zones have sharp boundaries and are thought to relate to several stages of growth, and potentially metamorphic events.

The garnet core (Zone I, similar to to Grt 1 in Rollinson 2002) in samples G12/101 and G12/113 is Fe and Ca-poor. It yields decreasing Mn and HREE contents that are coherent with Rayleigh-fractionation during continuous growth. The marked negative Eu anomaly is indication for plagioclase presence during garnet growth. The core inclusions show a straight layering or foliation, which suggests no rotational deformation during its growth. As an indication, Boak & Dymek (1982) calculated garnet-biotite temperatures of 583 ±30 and 542 ±20°C for garnet cores from two samples of schists with a similar assemblage and from the same unit of the investigated samples; however, this temperature was calculated using matrix biotite compositions that might have been reset during subsequent metamorphic events, moreover, the internal zoning of the garnet was not precisely documented. The growth of the garnet core is thus ascribed to prograde growth in a plagioclase bearing assemblage at amphibolite facies.

Two Ca-rich mantles (Zone II and III) surround the garnet core. These mantles have a sharp contact with the core. In G12/101, the Ca-rich mantles are depleted outwards in HREE and Mn. In G12/113, the HREE become depleted and then enriched, in an oscillatory pattern that resembles what is seen in Ca, and are likely due to concurring mineral reactions involving HREE-rich phases (Moore et al. 2013). Garnet zones of similar composition were reported by Rollinson (2003) as oscillatory zoned Garnet 2. Rollinson (2002) calculated temperatures of between 570 and 650°C for early Garnet 2. The increased Ca in garnet is commonly interpreted as the sign of increased pressure (Rollinson 2002; Rollinson 2003). This record of increased pressure is in line with the presence of kyanite is some B2 samples (Boak and Dymek 1982), for which a minimal pressure of 6 kbar was estimated. In G12/113 and other staurolite-bearing layers, the Ca-rich garnet rims seem texturally contemporaneous to staurolite porphyroblasts (now partially replaced by pseudomorphs) that deflect the main foliation. These Ca-rich mantles yield no Eu anomaly in both samples, which suggests that the coexisting assemblage was plagioclase-poor or absent. Absence of plagioclase is consistent with higher pressures, as plagioclase can react to form epidote-group minerals and amphibole at higher P conditions. The Ca-rich mantle is thus interpreted as grown in

504 medium/high-P amphibolite conditions typical of Barrovian-type metamorphism associated
505 with tectonic crustal thickening.

506 The outer Mg-rich and Ca-poor rim (Zone IV) of the garnet has a higher Mg# that
507 corresponds to what reported by Rollinson (2003) for his Garnet 3. For this growth zone
508 Rollinson (2002) calculated garnet-biotite T of ca. 530°C (490-534°C). Recalculated T from
509 the data in Boak and Dymek (1982) yields. 487-516 °C and 480-509°C for garnet rim and
510 adjacent biotite pairs in two samples (using the same calibration of Perchuk and Lavrent'eva
511 1983, for a range of P = 1 kbar to P = 6 kbar). In sample G12/101, the garnet rim yields a
512 negative Eu anomaly, whereas garnet rim in G12/113 does not show a Eu anomaly. This
513 difference reflects the bulk chemistry and in turn the matrix mineralogy: G12/101 yields 40
514 mode % of plagioclase and is relatively garnet poor, whereas sample G12/113 is poorer in Ca
515 and Na and it contains abundant garnet, but only minor plagioclase. The garnet rim appears to
516 grow statically on the previous foliation, and it is not present where quartz-filled pressure
517 shadows are located. It grows over staurolite pseudomorphs in G12/113 and occasionally
518 yields chloritoid inclusions that grow at the expanse of staurolite relicts, as seen in the matrix
519 (Figure 2b, Figure 3a). The matrix minerals plagioclase and chloritoid and the absence of
520 staurolite are indicative of upper greenschist to lower amphibolite facies, in line with
521 previous estimates of 450-530°C for garnet rim growth (Rollinson 2002; Boak and Dymek,
522 1982).

523 ## 4.4 Tectonic significance of garnet-growth zones

524 The garnet zoning is consistent with growth during different metamorphic stages at low and
525 high-P geotherms. This evolution cannot be reconciled with prograde to retrograde evolution
526 along a single P-T path (e.g. Komiya et al., 2002), but requires overprinting tectono-
527 metamorphic events.

528 The chemistry of B2 schists garnet cores is specific to the tectonic slice containing the B2
529 unit, and has not been detected in garnet anywhere else in the Isua supracrustal belt
530 (Rollinson 2002). The growth of the cores thus indicates a first prograde metamorphism
531 before the assembly of the 3700 Ma package subdomains. A plausible tectonic setting for the
532 formation of the garnet cores would be high heat-flow metamorphism, shortly after
533 deposition of the B2 mafic schists in the environment described by Nutman et al. (2015b).

The temperature for garnet core and mantle growth (with the presence of staurolite) is higher than what is recorded in the metamorphosed Ameralik dykes that crosscut the Isua supracrustal belt (intruded at 3500 Ma, maximal temperature of metamorphic equilibration of around 550°C, Rollinson 2002). This higher recorded temperature demonstrates that garnet Zones I to III grew during Eoarchaean, before 3500 Ma. This mid–high P metamorphism and deformation can be correlated to a crustal thickening event during the 3690-3660 assembly of the 3700 and the 3800 Ma packages: the Itsukasian orogeny described by Nutman et al. (2015b). Crust-stacking was followed by extensional high-heat flow pan-Itsaq Gneiss Complex metamorphism at ca. 3600 Ma (Nutman et al. 2014; Nutman et al. 2015c). In absence of direct dating of the garnet, the chronology of the crust-stacking and extensional events has been established on the basis of (i) cross-cutting relationships (see summary in Nutman and Friend, 2009), (ii) rare relicts of high-pressure granulites with an age of 3660 Ma, present within the gneisses north of the Isua supracrustal belt (Nutman et al. 2014; Nutman et al. 2015c) (iii) titanite and zircon ages of 3630–3620 Ma for amphibolite-facies metamorphism (Crowley and Myers 2002; Crowley 2003).

The lower grade conditions recorded in the garnet outer rim corresponds to conditions observed widely in the Isua Supracrustal Belt (Garnet 3 in most tectonic zones of Rollinson 2002), including the upper greenschist-lower amphibolite metamorphic facies overprinting the Ameralik dykes (Nutman, 1986, Rollinson, 2002). The outer garnet rim in the B2 schists records a lower temperature than recorded by the inner zones of the garnet (garnet-biotite temperature of 650°C in Rollinson 2002, and presence of staurolite). Formation of garnet on the retrograde path is not expected in Barrovian metamorphism of metapelites. It is thus likely that this zone formed during a separate tectonic event whose peak temperature was lower. This inference is supported by the textural evidence that the garnet rim grew statically over a pre-existing higher T foliation, and over staurolite pseudomorphs after staurolite retrogression. We speculate that the garnet rim corresponds to the late Archaean metamorphic event in the uppermost greenschist facies to lower amphibolite facies experienced by the Itsaq complex. In Isua, the most significant post Ameralik dyke metamorphism occurred at ca. 2690 Ma (e.g. Nutman et al. 2015b and references therein).

4.5 Tracking WR $\delta^{18}O$ through geologic time

Garnet $\delta^{18}O$ values allow tracking back the whole-rock signature through geologic time. It has been shown that diffusivity of oxygen in garnet during metamorphism is negligible to T of at least 600°C (Page et al. 2014; Rubatto and Angiboust 2015) and it oxygen isotopic signature may be retained up to 800°C (e.g. Vielzeuf et al. 2005, Higashino et al. 2019). G12/101 and G12/113 schists contain metamorphic garnet with $\delta^{18}O$ values of +8.7 to +9.7 ‰ that are significantly higher than the $\delta^{18}O$ values of +5.4 ±0.4‰ for magmatic zircon in felsic rock G04/46 (oxygen isotope fractionation between zircon and almandine garnet at T >500°C is <0.12‰, based on fractionation factors of Valley et al., 2003). All garnet zones, in both mafic samples (and the few indicative analyses in G04/46) yield similar high $\delta^{18}O$ values (9.5 ± 1 ‰). The single zircon rim measured at 10.1‰ in G04/46 could speculatively represent minor metamorphic zircon dissolution-reprecipitation, in equilibriumwith the garnet bearing assemblage.

Calculations confirm that that the measured bulk rock $\delta^{18}O$ value is in equilibrium with the measured garnet oxygen composition, and it has not been affected by post-metamorphic alteration. A simple model was calculated (*Supplementary material 8*) at temperatures of 500, 550 and 610 °C(Boak and Dymek, 1982; Rollinson 2002), the modal composition for the 5 major minerals in each sample and oxygen fractionation factors from Zheng (1993a, 1993b). For G12-101, the modelled $\delta^{18}O$ WR-values in equilibrium with the four garnet zones vary between ca. +11.2 and +11.5 ‰, in agreement with the measured bulk rock value of +11.6 ‰ (reported in Nutman et al. 2017). For G12-113, the modelled $\delta^{18}O$ values vary from ca. +11.2 to +11.7 ‰, again matching the measured bulk rock value of 11.5 ‰ (reported in Nutman et al. 2017). This agreement demonstrates that sample G12-101 and G12-113 remained a closed system for oxygen isotopes since the growth of the first garnet zone. The minor $\delta^{18}O$ decrease between measured values of garnet zone III and IV (-0.4 ‰ in G12-101 and -0.7 ‰ in G12-113) is at the limit of our analytic precision. The calculated model shows that a $\delta^{18}O$ decrease of this magnitude in garnet is expected for a minor decrease in temperature in a closed system (from >600°C down to 500°C), and does not require the input of external fluids. The result is similar to the model of Kohn et al. (1993) that predicts a variation in garnet $\delta^{18}O$ of ca. 1‰ over 100°C for metapelites.

593 The results implies that the Isua B2 metasedimentary rocks had acquired their high $\delta^{18}O$
594 values at the surface, and transported this $\delta^{18}O$ signature in the Archean crust before early
595 mid temperature metamorphism at ca. 3660-3690 Ma (age attributed to the garnet cores, see
596 above), and certainly before 3500 Ma (age of lower grade cross-cutting Ameralik dykes)
597 (Figure 11). Metamorphism of these sediments followed within 10 to 50 My of
598 sedimentation, which demonstrates the possibility for early and fast recycling of surficial
599 oxygen isotope signatures in the early Archean crust. The same process is recorded in the
600 Archaean high-grade metasedimentary rocks of the Pilbara, Australia (François et al. 2014)
601 and in the felsic meta-igneous crust of the Saglek Block in the North Atlantic Craton (Vezinet
602 et al. 2019). In contrast to previously identified high $\delta^{18}O$ Eoarchean lithologies such as
603 refractory BIFs and dolomites or low-volume altered horizons (3800 Ma Isua package
604 weathered volcanics, Nutman et al. 2015a) and thin sedimentary layers (e.g. Akilia
605 association metasedimentary rocks, Cates and Mojzsis, 2006), these rocks provide a
606 volumetrically important fertile source for high $\delta^{18}O$ crustal magmas (undiluted +12 ‰).
607 Melting of these sedimentary rocks can explain high $\delta^{18}O$ zircon grains as the result of S-type
608 granite formation early in Earth's history (e.g., Mojzsis et al. 2001; Peck et al. 2001; Trail et
609 al. 2007).

610 Many tectonic models that have been proposed for the Isua belt on the basis of structural and
611 petrographic studies are akin to modern subduction (e.g., Komiya et al. 1999; Hayashi et al.
612 2000; Arai et al. 2014) or flat subduction (Friend and Nutman 2005; Nutman et al. 2014;
613 Nutman et al. 2015c; Kaczmarek et al. 2016) followed by collisional orogeny. The latter
614 subduction model is in agreement with the observations here, and where relatively fast burial
615 to mid- to lower-crustal depth is facilitated during orogeny, as slivers of arc crust are
616 juxtaposed and stacked.

617

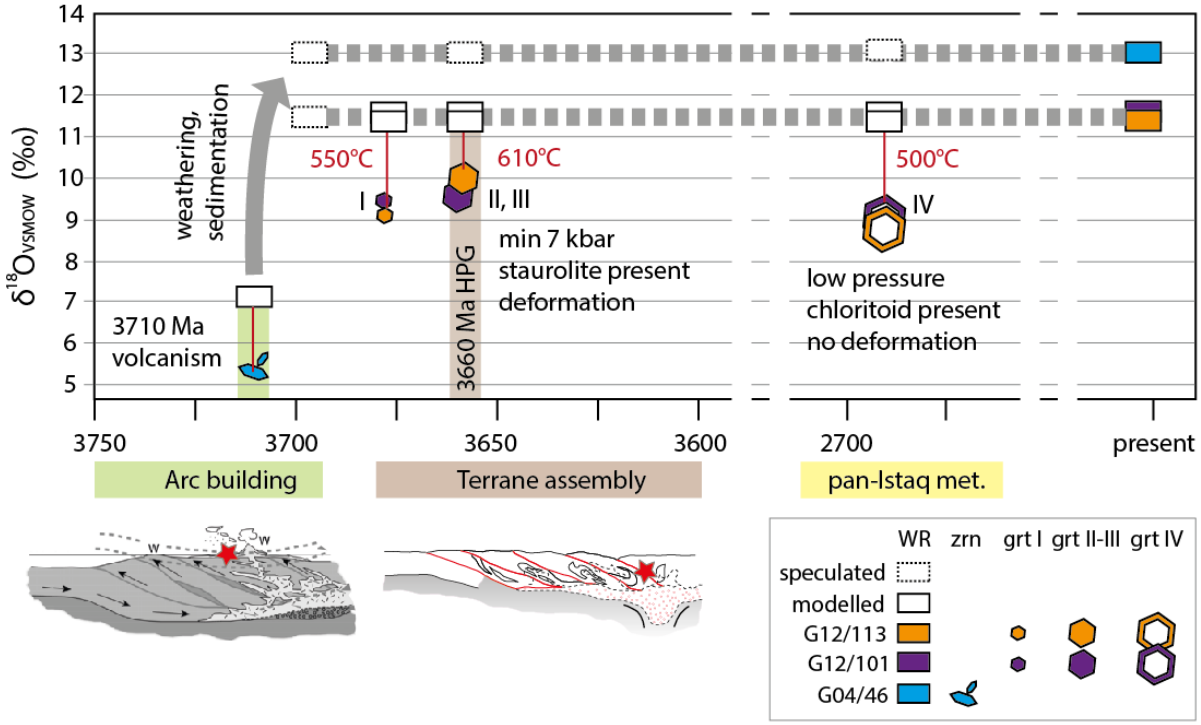

Figure 11. Summary of $\delta^{18}O$ data for B2 schists on the timeline of tectonic events in the Isua Supracrustal Belt. Measured zircon and garnet values are represented by filled symbols. Red lines show equilibrium relationships between measured minerals and modelled bulk rock at the temperatures shown in red. Sketch for arc building is taken from Nutman et al. (2013), and for terrane assembly including formation of a high-pressure granulite (HPG) from Nutman et al. (2015c). Red stars indicate the position of B2 schists at the different stages. ***(2 columns)***

5 Conclusions

1) 3700 Ma volcano-sedimentary rocks of the Isua supracrustal represent surficial lithologies with an elevated $\delta^{18}O$. Their elevated $\delta^{18}O$ value was acquired on the surface from low-temperature alteration such as weathering of mantle-derived 3700 – 3710 Ma arc rocks.

2) The alteration is marked by the offset between $\delta^{18}O$ values in 3709 Ma zircon that record the magmatic signature (ca. +5.3 ‰) and the whole rock $\delta^{18}O$ values (ca. +12 ‰).

3) The low temperature whole rock signature is inherited by garnet with $\delta^{18}O$ values of +8.7 to +9.7 ‰ and that records several phases of Archean metamorphism, including the crustal

634 stacking event that buried these lithologies to amphibolite facies conditions estimated to have
635 occurred at 3660 to 3650 Ma.

636 4) The combined $\delta^{18}O$ values of the metasedimentary whole rocks and the zircon and garnet
637 they contain require that the mafic protoliths crystallised from a mantle source, experienced
638 low temperature alteration/weathering to acquire elevated $\delta^{18}O$, and were buried to mid-
639 crustal levels forming high $\delta^{18}O$ garnet in a short period of time- within 10-50 My

640 5) Such crustal recycling occurring where temperatures reached partial melting, could have
641 produced Eoarchaean and potentially Hadean high $\delta^{18}O$ magmatic zircon within tens of
642 millions of years after the formation of the surficial lithologies.

643 ## Acknowledgements

644 Jörg Hermann, Jade-Star Lackey, Axel Schmitt, an anonymous reviewer and three
645 anonymous thesis examiners are thanked for constructive comments. Pierre Lanari kindly
646 assisted the production of EPMA maps. This work was funded by ARC projects
647 DP120100273 and DP170100715. DR acknowledges the support of ARC grant
648 DP110101599 and SNSF grant 200021-166280.
649

References

Appel PWU, Fedo CM, Moorbath S, Myers J (1998) Recognizable primary volcanic and sedimentary features in a low-strain domain of the highly deformed, oldest known (~ 3.7-3.8 Gyr) Greenstone Belt, Isua, West Greenland. Terra Nov 10:57–62. doi: 10.1046/j.1365-3121.1998.00162.x

Arai T, Omori S, Komiya T, Maruyama S (2014) Intermediate P/T-type regional metamorphism of the Isua Supracrustal Belt, southern west Greenland: The oldest Pacific-type orogenic belt? Tectonophysics 662:22–39. doi: 10.1016/j.tecto.2015.05.020

Baadsgaard H, Nutman AP, Rosing MT, et al (1986) Alteration and metamorphism of Amitsoq gneisses from the Isukasia area, West Greenland: Recommendations for isotope studies of the early crust. Geochim Cosmochim Acta 50:2165–2172. doi: http://dx.doi.org/10.1016/0016-7037(86)90071-2

Blichert-Toft J, Frei R (2001) Complex Sm-Nd and Lu-Hf isotope systematics in metamorphic garnets from the Isua supracrustal belt, West Greenland. Geochim Cosmochim Acta 65:3177–3189. doi: http://dx.doi.org/10.1016/S0016-7037(01)00680-9

Boak J, Dymek RF (1982) Metamorphism of the ca. 3800 Ma supracrustal rocks at Isua, West Greenland: implications for early Archaean crustal evolution. Earth Planet Sci Lett 59:155–176. doi: http://dx.doi.org/10.1016/0012-821X(82)90123-6

Bolhar R, Kamber BS, Moorbath S, et al (2004) Characterisation of early Archaean chemical sediments by trace element signatures. Earth Planet Sci Lett 222:43–60. doi: 10.1016/j.epsl.2004.02.016

Bolhar R, Kamber BS, Moorbath S, et al (2005) Chemical characterization of earth's most ancient clastic metasediments from the Isua Greenstone Belt, southern West Greenland. Cosmochim Acta 69:1555–1573.

Cates NL, Mojzsis SJ (2006) Chemical and isotopic evidence for widespread Eoarchean metasedimentary enclaves in southern West Greenland. Geochim Cosmochim Acta 70:4229–4257. doi: 10.1016/j.gca.2006.05.014

Crowley JL (2003) U-Pb geochronology of 3810-3630 Ma granitoid rocks south of the Isua greenstone belt, southern West Greenland. Precambrian Res 126:235–257. doi: 10.1016/s0301-9268(03)00097-4

Crowley JL, Myers J (2002) Timing and nature of multiple 3700–3600 Ma tectonic events in intrusive rocks north of the Isua greenstone belt, southern West Greenland.

Dymek RF, Boak J, Gromet L (1983) Average sedimentary rock rare Earth element patterns and crustal evolution: Some observations and implications from the 3800 Ma ISUA supracrustal belt, West Greenland.

Ferry JM, Kitajima K, Strickland A, Valley JW (2014) Ion microprobe survey of the grain-scale oxygen isotope geochemistry of minerals in metamorphic rocks. Geochim Cosmochim Acta 144:403–433. doi: 10.1016/j.gca.2014.08.021

Ferry JM, Spear FS (1978) Experimental calibration of the partitioning of Fe and Mg between biotite and garnet. Contrib to Mineral Petrol 66:113–117. doi: 10.1007/BF00372150

François C, Philippot P, Rey PF, Rubatto D (2014) Burial and exhumation during Archean sagduction in the East Pilbara Granite-Greenstone Terrane. Earth Planet Sci Lett 396:235–251. doi: 10.1016/j.epsl.2014.04.025

Friend CRL, Nutman AP (2005) Complex 3670–3500 Ma orogenic episodes superimposed on juvenile crust accreted between 3850 and 3690 Ma, Itsaq Gneiss Complex, southern West Greenland.

Furnes H, de Wit M, Staudigel H, et al (2007) A vestige of Earth's oldest ophiolite. Science (80-) 315:1704–1707. doi: 10.1126/science.1139170

Gauthiez-Putallaz L, Rubatto D, Hermann J (2016) Dating prograde fluid pulses during subduction by in situ U-Pb and oxygen isotope analysis. Contrib to Mineral Petrol 171:1–20. doi: 10.1007/s00410-015-1226-4

Gregory RT, Taylor HP (1981) An oxygen isotope profile in a section of Cretaceous oceanic crust, Samail Ophiolite, Oman: Evidence for δ18O buffering of the oceans by deep (>5 km) seawater-hydrothermal circulation at mid-ocean ridges. J Geophys Res Solid Earth 86:2737–2755. doi: 10.1029/JB086iB04p02737

Gruau G, Rosing MT, Bridgwater D, Gill R (1996) Resetting of Sm -- Nd systematics during metamorphism of > 3.7-Ga rocks: implications for isotopic models of early Earth differentiation. Chem Geol 133:225–240. doi: 10.1016/S0009-2541(96)00092-7

Hayashi M, Komiya T, Nakamura Y, Maruyama S (2000) Archean Regional Metamorphism of the Isua Supracrustal Belt, Southern West Greenland: Implications for a Driving Force for Archean Plate Tectonics. Int Geol Rev 42:1055–1115. doi: 10.1080/00206810009465128

Hiess J, Bennett VC, Nutman AP, Williams IS (2009) In situ U–Pb, O and Hf isotopic compositions of zircon and olivine from Eoarchaean rocks, West Greenland: New insights to making old crust. Geochim Cosmochim Acta 73:4489–4516.

Hiess J, Bennett VC, Nutman AP, Williams IS (2011) Archaean fluid-assisted crustal cannibalism recorded by low δ18O and negative εHf(T) isotopic signatures of West Greenland granite zircon. Contrib to Mineral Petrol 161:1027–1050. doi: 10.1007/s00410-010-0578-z

Higashino F, Rubatto D, Kawakami T, Bouvier A-S, Baumgartner LP (2019) Oxygen isotope speedometry in granulite facies garnet recording fluid/melt–rock interaction (Sør Rondane Mountains, East Antarctica). J Metamorph Geol 37:1037-1048.

Hoskin PWO, Schaltegger U (2003) The composition of zircon and igneous and metamorphic petrogenesis. Rev Mineral geochemistry 53:27–62.

Kaczmarek M-A, Reddy SM, Nutman AP, et al (2016) Earth's oldest mantle fabrics indicate Eoarchaean subduction. Nat Commun 7:10665. doi: 10.1038/ncomms10665

Kamber BS, Whitehouse MJ, Bolhar R (2005) Volcanic resurfacing and the early terrestrial crust: zircon U–Pb and REE constraints from the Isua Greenstone Belt, southern West Greenland. Earth Planet 240:276–290.

Kohn MJ (1993) Modeling of prograde mineral δ18O changes in metamorphic systems. Contrib to Mineral Petrol 113:249–261.

Kohn MJ, Valley JW, Elsenheimer D, Spicuzza MJ (1993) O isotope zoning in garnet and staurolite: evidence for closed- system mineral growth during regional metamorphism. Am. Mineral. 78:988–1001.

Komiya T, Hayashi M, Maruyama S, Yurimoto H (2002) Intermediate-P/T type Archean metamorphism of the Isua supracrustal belt: Implications for secular change of geothermal gradients at subduction zones and for Archean plate tectonics. Am J Sci 302:806–826. doi: 10.2475/ajs.302.9.806

Komiya T, Maruyama S, Masuda T, et al (1999) Plate tectonics at 3.8-3.7 Ga: field evidence from the Isua accretionary complex, southern West Greenland. J 107:515–554. doi: 10.1086/314371

Lanari P, Burn M, Loury C, et al (2014) XMapTools a program for X-ray images processing and thermobarometric studies. Geophys Res Abstr. doi: doi.org/10.1103/PhysRevB.82.161108

Lanari P, Guillot S, Schwartz S, et al (2012) Diachronous evolution of the alpine continental subduction wedge: Evidence from P-T estimates in the Briançonnais Zone houillère (France - Western Alps). J Geodyn 56–57:39–54. doi: 10.1016/j.jog.2011.09.006

Lanari P, Riel N, Guillot S, et al (2013) Deciphering high-pressure metamorphism in collisional context using microprobe mapping methods: Application to the Stak eclogitic massif (northwest Himalaya). Geology 41:111–114. doi: 10.1130/G33523.1

Lawrence J, Taylor HP (1971) Deuterium and oxygen-18 correlation: Clay minerals and hydroxides in Quaternary soils compared to meteoric waters.

Ludwig K (2009) SQUID 2 (rev. 2.50): A User's Manual Berkeley Geochronology Center Spec Pub 5:104p

Ludwig KR (2012) User's Manual for Isoplot 3.75. A Geochronological Toolkit for Microsoft Excel. Berkeley Geochronol Center Spec Pub 5:75p.

Martin LAJ, Rubatto D, Crépisson C, et al (2014) Garnet oxygen analysis by SHRIMP-SI: Matrix corrections and application to high-pressure metasomatic rocks from Alpine Corsica. Chem Geol 374–375:25–36. doi: 10.1016/j.chemgeo.2014.02.010

Mojzsis SJ, Harrison TM, Pidgeon RT (2001) Oxygen-isotope evidence from ancient zircons for liquid water at the Earth's surface 4,300 Myr ago. Nature 409:178–181. doi: 10.1038/35051557

Nutman AP (1986) The early Archaean to Proterozoic history of the Isukasia area, Southern West Greenland. Bulletin of the Geological survey of Greenland 154 80pp.

Nutman AP, Allaart JH, Bridgwater D, et al (1984) Stratigraphic and geochemical evidence for the depositional environment of the early archaean isua supracrustal belt, southern west greenland. Precambrian Res 25:365–396. doi: 10.1016/0301-9268(84)90010-X

Nutman AP, Collerson KD (1991) Very early Archean crustal-accretion complexes preserved in the North Atlantic Craton. Geology 19: 791-795.

759 Nutman AP, Bennett VC, Friend CRL, McGregor VR (2000) The early Archaean Itsaq Gneiss Complex of
760 Southern West Greenland: the importance of field observations in interpreting age and isotopic
761 constraints for early terrestrial evolution. Geochimica Cosmochimica Acta 64: 3035-3060.
762 Nutman AP, Bennett VC, Friend CRL, Hidaka, H, Yi K, Lee SR, Kamiichi T. (2013) Episodic 3920-3660
763 Ma juvenile crust formation and 3660-3600 Ma recycling in the Itsaq Gneiss Complex of southern
764 West Greenland. American Journal of Science 313: 877-911. doi: 10.2475/09.2013.00
765 Nutman AP, Bennett VC, Chivas AR, et al (2015a) 3806Ma Isua rhyolites and dacites affected by low
766 temperature Eoarchaean surficial alteration: Earth's earliest weathering. Precambrian Res
767 268:323–338. doi: 10.1016/j.precamres.2015.07.014
768 Nutman AP, Bennett VC, Friend CRL (2015b) The emergence of the Eoarchaean proto-arc: Evolution of a
769 c. 3700 Ma convergent plate boundary at Isua, southern West Greenland.
770 Nutman AP, Bennett VC, Friend CRL (2015c) Proposal for a continent "Itsaqia" amalgamated at 3.66 Ga
771 and rifted apart from 3.53 Ga: Initiation of a Wilson cycle near the start of the rock record. Am J
772 Sci 315:509–536. doi: 10.2475/06.2015.01
773 Nutman AP, Bennett VC, Friend CRL, et al (2014) The itsaq gneiss complex of greenland: Episodic 3900
774 to 3660 Ma juvenile crust formation and recycling in the 3660 to 3600 Ma Isukasian orogeny. Am
775 J Sci. doi: 10.2475/09.2013.03
776 Nutman AP, Bennett VC, Friend CRL, Chivas AR (2017) The Isua Supracrustal Belt of the North Atlantic
777 Craton (Greenland). In: Sediment Provenance. Elsevier, pp 563–592
778 Nutman AP, Bennett VC, Friend CRL, Van Kranendonk M, Chivas AR (2019) Reconstruction of a 3700
779 Ma transgressive marine environment from Isua (Greenland): Sedimentology, stratigraphy and
780 geochemical signatures. Lithos DOI: 10.1016/j.lithos.2019.105164.
781 Nutman AP, Bennett VC, Friend CRL, Rosing MT (1997) ~ 3710 and ⩾ 3790 Ma volcanic sequences in
782 the Isua (Greenland) supracrustal belt; structural and Nd isotope implications. Chem Geol
783 141:271–287. doi: http://dx.doi.org/10.1016/S0009-2541(97)00084-3
784 Nutman AP, Bridgwater D (1986) Early Archaean Amitsoq tonalites and granites of the Isukasia area,
785 southern West Greenland: development of the oldest-known sial.
786 Nutman AP, Friend CRL (2009) New 1:20,000 scale geological maps, synthesis and history of
787 investigation of the Isua supracrustal belt and adjacent orthogneisses, southern West Greenland: A
788 glimpse of Eoarchaean crust formation and orogeny. Precambrian Res 172:189–211. doi:
789 McGregor VR (1973) The early Precambrian gneisses of the Godthåb district, West Greenland:
790 Philosophical Transactions of the Royal Society of London A273: 343-358.Moore SJ, Carlson
791 WD, Hesse MA (2013) Origins of yttrium and rare earth element distributions in metamorphic
792 garnet. J Metamorphic Geol 31(6):663-689 doi:10.1111/jmg.12039
793 Page FZ, Essene EJ, Mukasa SB, Valley JW (2014) A garnet-zircon oxygen isotope record of subduction
794 and exhumation fluids from the Franciscan complex, California. J Petrol 55:103–131. doi:
795 10.1093/petrology/egt062Paton C, Hellstrom J, Paul B, et al (2011) Iolite: Freeware for the
796 visualisation and processing of mass spectrometric data. J Anal At Spectrom 26:2508–2518. doi:
797 10.1039/c1ja10172b
798 Peck WH, Valley JW, Wilde SA, Graham CM (2001) Oxygen isotope ratios and rare earth elements in 3.3
799 to 4.4 Ga zircons: Ion microprobe evidence for high ??18O continental crust and oceans in the
800 early Archean. Geochim Cosmochim Acta 65:4215–4229. doi: 10.1016/S0016-7037(01)00711-6
801 Perchuk LL, Lavrent'eva I V. (1983) Experimental Investigation of Exchange Equilibria in the System
802 Cordierite-Garnet-Biotite. Springer New York, pp 199–239
803 Perry E, Ahmad S, Swulius T (1978) The oxygen isotope composition of 3,800 my old metamorphosed
804 chert and iron formation from Isukasia, West Greenland.
805 Polat A, Hofmann A, Rosing MT (2002) Boninite-like volcanic rocks in the 3.7–3.8 Ga Isua greenstone
806 belt, West Greenland: geochemical evidence for intra-oceanic subduction zone processes in the
807 early. Chem Geol 184:231–254. doi: 10.1016/S0009-2541(01)00363-1
808 Pope ECE, Bird DK, Rosing MT (2012) Isotope composition and volume of Earth's early oceans. Proc
809 Natl Acad Sci U S A 109:4371–4376. doi: 10.1073/pnas.1115705109
810 Rollinson H (2002) The metamorphic history of the Isua Greenstone Belt, West Greenland. Geol Soc
811 London, Spec Publ 199:329–350. doi: 10.1144/GSL.SP.2002.199.01.16
812 Rollinson H (2003) Metamorphic history suggested by garnet-growth chronologies in the Isua Greenstone
813 Belt, West Greenland. In: Precambrian Research. pp 181–196
814 Rose N, Rosing MT, Bridgwater D (1996) The origin of metacarbonate rocks in the Archaean Isua
815 supracrustal belt, West Greenland. Am J Sci 296:1004–1044. doi: 10.2475/ajs.296.9.1004

816 Rosing MT (1999) 13C-Depleted Carbon Microparticles in >3700-Ma Sea-Floor Sedimentary Rocks from
817 West Greenland. Science (80-) 283:674–676. doi: 10.1126/science.283.5402.674
818 Rubatto D, Angiboust S (2015) Oxygen isotope record of oceanic and high-pressure metasomatism: a P–
819 T–time–fluid path for the Monviso eclogites (Italy). Contrib to Mineral Petrol 170:44. doi:
820 10.1007/s00410-015-1198-4
821 Savin SM, Epstein S (1970) The oyxgen and hydrogen isotope geochemistry of ocean sediments and
822 shales. Geochim Cosmochim Acta 34:43–63. doi: 10.1016/0016-7037(70)90150-X
823 Sheppard S, Gilg H, Sheppard, S. M. F., Gilg H a. (1996) Stable isotope geochemistry of clay minerals.
824 Clay Miner 31:1–24.
825 Stacey JS t, Kramers J (1975) Approximation of terrestrial lead isotope evolution by a two-stage model.
826 Earth Planet Sci Lett 26:207–221.
827 Sun S-S, McDonough WF (1989) Chemical and isotopic systematics of oceanic basalts: implications for
828 mantle composition and processes. Geol Soc London, Spec Publ 42:313–345.
829 Thébauda N, Rey PF (2013) Archean gravity-driven tectonics on hot and flooded continents: Controls on
830 long-lived mineralised hydrothermal systems away from continental margins. Precambrian Res
831 229:93–104. doi: 10.1016/j.precamres.2012.03.001
832 Trail D, Mojzsis SJ, Harrison TM, et al (2007) Constraints on Hadean zircon protoliths from oxygen
833 isotopes, Ti-thermometry, and rare earth elements. Geochemistry, Geophys Geosystems. doi:
834 10.1029/2006GC001449
835 Valley JW, Bindeman IN, Peck WH (2003) Empirical calibration of oxygen isotope fractionation in zircon.
836 Geochim Cosmochim Acta 67:3257–3266. doi: 10.1016/S0016-7037(00)00090-5
837 Valley JW, Kinny PD, Schulze DJ, Spicuzza MJ (1998) Zircon megacrysts from kimberlite: oxygen
838 isotope variability among mantle melts. Contrib to Mineral Petrol 133:1–11. doi:
839 10.1007/s004100050432
840 Valley JW, Kitchen N, Kohn MJ, et al (1995) UWG-2, a garnet standard for oxygen isotope ratios:
841 Strategies for high precision and accuracy with laser heating. Geochim Cosmochim Acta 59:5223–
842 5231. doi: http://dx.doi.org/10.1016/0016-7037(95)00386-X
843 Vezinet, A., Thomassot E, Pearson DG, Stern RA, Luo Y, Sarkar C., 2019. Extreme $\delta^{18}O$ signatures in
844 zircon from the Saglek Block (North Atlantic Craton) document reworking of mature supracrustal
845 rocks as early as 3.5 Ga. Geology, 47(7): 605-608, doi:10.1130/g46086.1
846 Vielzeuf D, Veschambre M, Brunet F (2005b) Oxygen isotope heterogeneities and diffusion profile in
847 composite metamorphic-magmatic garnets from the Pyrenees. Am Mineral 90:463–472. doi:
848 10.2138/am.2005.1576
849 Whitney DL, Evans BW (2010) Abbreviations for names of rock-forming minerals. Am Mineral 95:185–
850 187. doi: 10.2138/am.2010.3371
851 Wilde SA., Valley JW, Peck WH and Graham CM, (2001), Evidence form detrital zircons for the
852 existence of continental crust and oceans 4.4 Ga ago, Nature, 409, 175– 178.
853 Williams IS (1998) U–Th–Pb geochronology by ion microprobe. Rev Econ Geol 7:1–35.
854 Woodhead JD, Hellstrom J, Hergt JM, et al (2007) Isotopic and elemental imaging of geological materials
855 by laser ablation inductively coupled plasma□mass spectrometry. Geostand Geoanalytical Res
856 31:331–343
857 Zheng Y-F (1993a) Calculation of oxygen isotope fractionation in anhydrous silicate minerals. Geochim
858 Cosmochim Acta 57:1079–1091.
859 Zheng Y-F (1993b) Calculation of oxygen isotope fractionation in hydroxyl-bearing silicates. Earth Planet
860 Sci Lett 120:247–263.
861

Supplementary material

Supplementary material 1. SHRIMP analyses of U-Pb in G04/46 zircons

Supplementary material 2. LA-ICP-MS analyses of trace elements in G04/46 zircons (osc: oscillatory zones)

Supplementary material 3. SHRIMP analyses of oxygen isotopes ($\delta^{18}O_{VSMOW}$) in G04/46 zircons

Supplementary material 4. EMPA XSps, XGrs and XAlm maps of G12/101 garnet set in SHRIMP mount. In white, indication of chemical zones (I, II, III, IV)

Supplementary material 5. EMPA XSps, XGrs and XAlm maps of G12/113 garnet set in SHRIMP mount. In white, indication of chemical zones (I, II, III, IV)

Supplementary material 6. LA-ICP-MS analyses of trace elements in G12/101 and G12/113 garnet

Supplementary material 7. SHRIMP analyses of oxygen isotopes ($\delta^{18}O_{VSMOW}$) in G12/101 and G12/113 garnet

Supplementary material 8. Whole-rock $\delta^{18}O$ modelling

					^{204}Pb corrected data												
Spot Name	CL	ppm U	ppm Th	^{232}Th /^{238}U	%c. ^{206}Pb	^{238}U /^{206}Pb*	% err	^{207}Pb* /^{206}Pb*	% err	^{207}Pb/^{206}Pb date	1σ err	% disc.	^{207}Pb* /^{235}U	% err	^{206}Pb* /^{238}U	% err	err corr
G0446-1	osc	246	145	0.61	0.01	1.289	3.0	0.3511	0.24	**3712**	**4**	+0	37.57	3.0	0.7760	3.0	0.997
G0446-3	osc	484	530	1.13	0.08	1.298	3.2	0.3495	0.18	**3705**	**3**	+1	37.13	3.2	0.7705	3.2	0.998
G0446-4	osc	227	169	0.77	0.03	1.274	2.9	0.3494	0.26	**3704**	**4**	-1	37.82	2.9	0.7851	2.9	0.996
G0446-6	osc	152	102	0.70	0.01	1.266	2.9	0.3519	0.32	**3715**	**5**	-1	38.33	2.9	0.7902	2.9	0.994
G0446-7	osc	490	494	1.04	0.05	1.320	2.7	0.3549	1.39	**3728**	**21**	+3	37.06	3.0	0.7574	2.7	0.889
G0446-8	osc	233	164	0.73	0.03	1.303	3.2	0.3504	0.27	**3709**	**4**	+1	37.06	3.2	0.7672	3.2	0.996
G0446-9	osc	119	86	0.75	0.26	1.270	1.1	0.3483	0.38	**3700**	**6**	-2	37.81	1.2	0.7873	1.1	0.946
G0446-10	osc	235	159	0.70	0.01	1.275	3.3	0.3530	0.25	**3720**	**4**	-0	38.16	3.3	0.7840	3.3	0.997
G0446-11	osc	291	263	0.93	0.00	1.289	2.9	0.3505	0.23	**3709**	**4**	+0	37.48	2.9	0.7757	2.9	0.997
Rejected discordant analyses																	
G0446-2	w	87	58	0.69	8.48	1.443	8.1	0.3406	4.59	**3666**	**70**	+10	32.54	9.3	0.6930	8.1	0.869
G0446-5	w	53	31	0.61	0.19	1.425	2.7	0.3377	0.55	**3652**	**8**	+8	32.67	2.8	0.7017	2.7	0.981

osc: oscillatory zone
w: white rim/zone
c.: common
disc.: discordant
err are 1σ

spot #	zirc28-02	zirc28-03	zirc28-05	zirc28-07	zirc28-08	zirc28-09	zirc28-10	zirc22-25	zirc22-27	zirc22-24	zirc22-29	zirc22-30
CL	osc	osc	osc	osc	osc	osc	osc	osc	osc	osc	osc	osc
(ppm)												
P	322	550	124	259	271	368	453	426	232	226	297	556
Ca	78	630	47	bdl	13	320	43	270	247	41	108	97
Sc	449	454	422	442	472	460	546	456	420	502	552	453
Ti	4	4	6	3	10	25	8	4	5	8	8	14
Fe	110	109	403	62	157	614	166	113	148	168	81	37
Y	1051	1568	900	972	2326	2182	4300	1542	1796	1224	1777	2556
Zr (wt%)	40.95	41.09	43.39	40.79	42.63	41.29	42.8	43.67	38.91	41.9	42.8	46.79
Nb	2.26	1.61	1.01	2.39	2.02	4.05	4.33	2.9	1.98	2.59	3	3.67
La	0.082	0.195	1.19	0.144	0.656	0.179	1.43	0.35	0.334	0.386	0.169	bdl
Ce	11.56	13.37	8.82	16.12	19.19	8.27	40.32	16.76	10.01	9.56	8.41	9.03
Pr	0.117	0.323	0.542	0.08	0.686	0.473	1.34	0.305	0.436	0.23	0.197	0.076
Nd	1.99	5.08	5.06	1.66	8.84	7.51	18.61	4.15	5.78	2.48	3.42	2.36
Sm	4.25	8.95	5.57	3.48	15.68	13.9	33.8	8.25	11.18	3.94	6.93	5.94
Eu	0.546	1.34	1.92	0.435	3.42	3.19	6.32	0.86	2.19	1.42	1.52	1.29
Gd	25.31	47.7	25.5	23.55	76.9	77.7	166.2	40.9	58.2	24.3	42.2	47.7
Tb	7.92	13.6	7.19	7.68	22.08	21.47	46.2	12.56	16.86	7.93	13.68	17.83
Dy	99.6	158.7	82	92.6	243.5	238.6	504	153.2	189.7	104.1	168.8	233.3
Ho	36.05	54.42	28.1	33.16	80.5	76.9	156.4	53.2	63	40.2	62	87.3
Er	172	244.1	134	155	355.4	342.9	677	246	275.7	201.7	283.7	416
Tm	33.01	45.25	27.9	30.21	67.3	62.3	119.3	47.6	51	41.4	54.04	83.3
Yb	313.5	408.6	270	271.6	580	543	1035	444	439	387	490.6	754
Lu	56.4	70.1	47.9	48.71	97.5	94.2	169.7	74.2	78.7	73.2	86.6	124.9
Hf	8830	8730	7970	9010	8110	7250	7680	9150	7355	7410	6620	8700
Ta	0.72	0.52	0.24	0.85	0.57	1.06	0.93	0.88	0.65	0.59	0.75	1.30
Pb	30	44	27	50	79	52	158	47	46	21	47	1.5
Th	75	108	66	122	194	124	408	121	107	56	125	77
U	130	142	74	175	199	168	318	181	141	115	173	71

Spot	zone	$^{18}O/^{16}O$	±2SE	$\delta^{18}O$ (‰)	±SE
G0446-9	osc	0.00204431	7.7E-08	5.17	0.04
G0446-4	osc	0.00204523	1.52E-07	5.62	0.07
G0446-1	osc	0.00204432	2.1E-07	5.18	0.10
G0446-2	osc	0.00204476	1.3E-07	5.39	0.06
G0446-3*	osc	0.00204281	2.42E-07	4.45	0.12
G0446-5	osc	0.00204500	1.28E-07	5.51	0.06
G0446-10	osc	0.00204471	1.45E-07	5.37	0.07
			Average:	**5.38**	
			Stdev:	**0.18**	
G0446-7	w	0.00204565	2.1E-07	5.83	0.10
G0446-8	w	0.00204657	1.25E-07	6.28	0.06
G0446-13	w	0.00204483	1.98E-07	5.43	0.10
G0446-12	w	0.00204425	1.2E-07	5.14	0.06
G0446-14	w	0.00204615	1.39E-07	6.07	0.07
G0446-6	w	0.00204384	1.44E-07	4.95	0.07
G0446-15	w	0.00204528	1.01E-07	5.65	0.05
			Average:	**5.62**	
			Stdev:	**0.48**	
G0446-11	w, fr	0.00205445	1.68E-07	10.12	0.08

* outlier rejected from average
osc: oscillatory zone
w: white rim/zone
fr: fracture

Instrument:	SHRIMP SI
Session:	17/03/14
TEM repeatability:	0.20

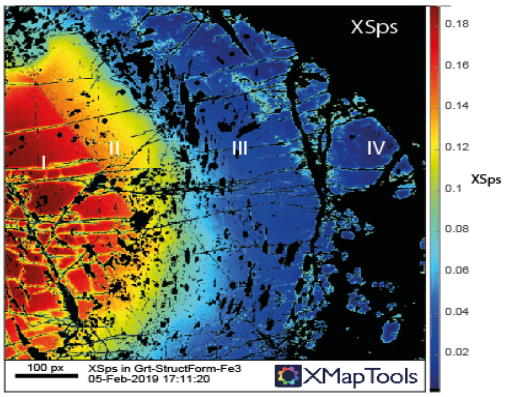
XSps
I
II
III
IV
0.18
0.16
0.14
0.12
0.1
0.08
0.06
0.04
0.02
XSps
100 px
XSps in Grt-StructForm-Fe3
05-Feb-2019 17:11:20
XMapTools

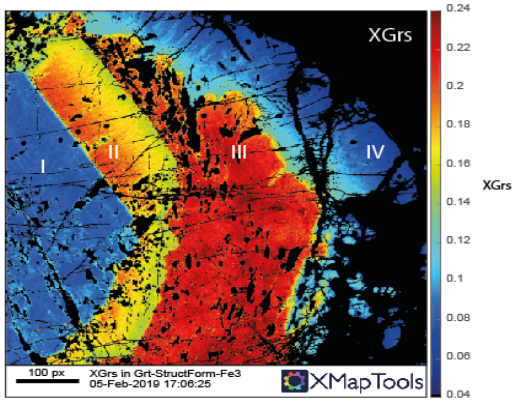
XGrs
I
II
III
IV
0.24
0.22
0.2
0.18
0.16
0.14
0.12
0.1
0.08
0.06
0.04
XGrs
100 px
XGrs in Grt-StructForm-Fe3
05-Feb-2019 17:06:25
XMapTools

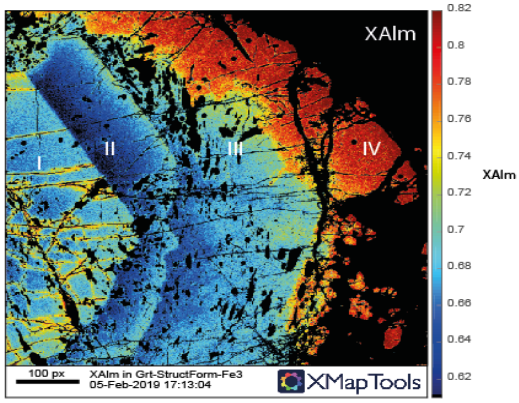
XAlm
I
II
III
IV
0.82
0.8
0.78
0.76
0.74
0.72
0.7
0.68
0.66
0.64
0.62
XAlm
100 px
XAlm in Grt-StructForm-Fe3
05-Feb-2019 17:13:04
XMapTools

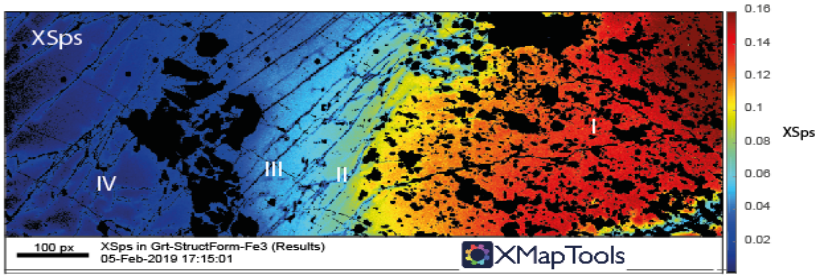
XSps
IV
III
II
I
100 px
XSps in Grt-StructForm-Fe3 (Results)
05-Feb-2019 17:15:01
XMapTools
0.16
0.14
0.12
0.1
0.08
0.06
0.04
0.02
XSps

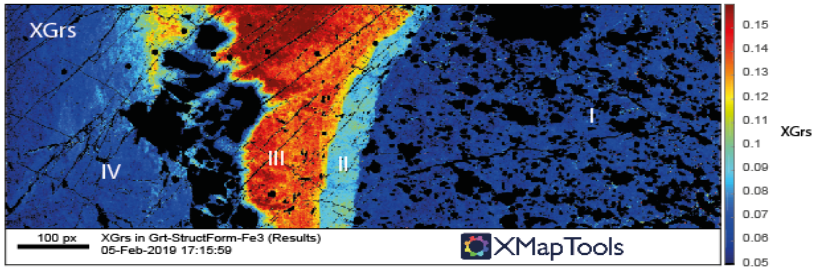
XGrs
IV
III
II
I
100 px
XGrs in Grt-StructForm-Fe3 (Results)
05-Feb-2019 17:15:59
XMapTools
0.15
0.14
0.13
0.12
0.11
0.1
0.09
0.08
0.07
0.06
0.05
XGrs

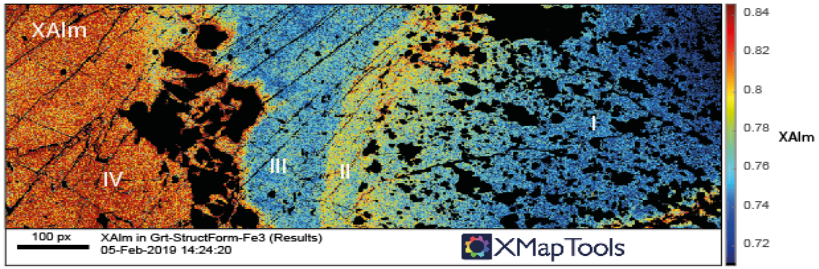
XAlm
IV
III
II
I
100 px
XAlm in Grt-StructForm-Fe3 (Results)
05-Feb-2019 14:24:20
XMapTools
0.84
0.82
0.8
0.78
0.76
0.74
0.72
XAlm

Sample	grt47_1 G12-113	grt47_2 G12-113	grt47_3 G12-113	grt47_4 G12-113	grt47_5 G12-113	grt47_6 G12-113	grt47_7 G12-113	grt47_8 G12-113	grt47_9 G12-113	grt47_10 G12-113	grt47_11 G12-113
Zone	I	I	I	I	I	II	II	III	III	III	III
(ppm)											
P	61.8	70.1	61	71.9	57.1	24.6	32.9	30.8	32.4	34.7	43.1
Ca (wt%)	1.366	1.328	1.309	1.345	1.207	2.492	2.834	3.47	3.289	2.488	2.637
Sc	124.2	152.5	178.1	144.4	111.7	107.3	167.3	197.4	199.9	218.2	163.4
Ti	229	293	258.5	316	167.5	57.8	135.3	232.1	190.1	204	207
Cr	1402	1676	2114	1829	1131	1536	2081	1871	1240	1357	1439
Mn	47770	52390	43360	36510	25790	17280	12630	10462	8214	6553	5585
Rb	0.774	0.428	bdl	bdl	bdl	0.085	bdl	0.316	bdl	0.088	0.224
Sr	0.287	0.142	0.032	bdl	bdl	bdl	bdl	bdl	bdl	0.044	0.027
Y	2699	1833	625.1	71.7	31.85	229.8	15.82	26.64	31.85	29.52	25.52
Zr	3.04	3.34	3.34	3.6	3.41	1.6	1.01	1.55	1.13	2.11	1.83
Nb	0.035	0.0091	0.028	bdl	0.022	bdl	bdl	0.0073	bdl	0.022	0.024
La	bdl	bdl	bdl	bdl	bdl	bdl	bdl	bdl	bdl	bdl	0.0168
Ce	bdl	bdl	0.0119	0.0148	bdl	bdl	bdl	bdl	bdl	bdl	0.073
Pr	0.0057	0.0074	0.007	0.0076	bdl	bdl	bdl	bdl	bdl	bdl	0.0078
Nd	0.168	0.197	0.235	0.379	0.23	bdl	bdl	0.052	bdl	bdl	0.064
Sm	2.56	3.65	4.96	3.96	2.69	0.156	0.303	0.324	0.385	0.331	0.525
Eu	0.306	0.383	0.463	0.584	0.485	0.581	0.687	0.836	0.81	0.588	0.779
Gd	53	68.5	59	16.66	9.21	3.6	3.57	3.51	3.66	3.12	3.93
Tb	24.59	24.43	13.58	2.26	1.289	2.19	0.775	0.75	0.722	0.714	0.757
Dy	298.7	233.3	93.9	12.7	6.64	27.64	3.38	4.73	5.44	5.41	5.21
Ho	92.32	60.78	17.84	2.25	0.992	6.72	0.411	0.861	1.225	1.199	0.992
Er	362.3	213.8	49.7	5.93	2.75	20.33	1.11	2.67	4.11	3.77	3.03
Tm	55.68	30.37	6.22	0.717	0.383	2.74	0.125	0.372	0.721	0.557	0.479
Yb	402.5	208.8	37.82	4.23	2.92	20.2	0.9	3.43	6.42	5.07	4.02
Lu	59.37	29.04	4.77	0.622	0.486	2.83	0.123	0.531	1.234	0.964	0.685
Hf	0.066	bdl	bdl	0.076	0.026	0.05	bdl	bdl	bdl	bdl	bdl
Ta	0.024	0.0229	0.0051	0.004	bdl	bdl	bdl	bdl	bdl	0.0051	bdl
Pb	bdl	0.035	bdl	bdl	bdl	0.082	bdl	0.88	0.089	0.81	0.86
Th	bdl	bdl	bdl	bdl	bdl	bdl	bdl	bdl	bdl	bdl	bdl
U	0.036	0.031	0.057	0.0176	bdl	bdl	bdl	bdl	bdl	bdl	bdl

Sample	grt47_12 G12-113	grt47_13 G12-113	grt47_14 G12-113	grt47_15 G12-113	grt47_16 G12-113	grt47_33 G12-101	grt47_34 G12-101	grt47_35 G12-101	grt47_36 G12-101	grt47_37 G12-101	grt47_38 G12-101
Zone	III	IV	IV	IV	IV	I	I	I	I	II	II
(ppm)											
P	39.1	50.9	69.7	84.2	116.6	62.8	57.7	67.2	50	28.1	29.7
Ca (wt%)	2.35	1.627	1.401	1.234	0.984	1.788	1.803	1.697	1.776	4.396	3.973
Sc	124.6	85.3	76.7	69.9	64.7	305.4	229.8	309	166.6	152.6	209.3
Ti	130	103.7	176.4	152.9	145.8	345	300.7	346.4	232.1	304.8	289
Cr	1628	1997	1983	1749	1260	539	420.1	411.9	239.3	347.6	555.1
Mn	4337	3250	1604	bdl	bdl	58160	50470	56520	46140	40790	35610
Rb	bdl	bdl	bdl	bdl	bdl	0.117	bdl	bdl	bdl	bdl	bdl
Sr	bdl	bdl	bdl	bdl	bdl	0.039	bdl	bdl	bdl	bdl	bdl
Y	52.6	bdl	bdl	bdl	bdl	591.5	238	184.8	305.1	109.6	59.47
Zr	1.72	2.03	4.28	7.5	6.51	4.03	3.08	3.97	2.65	0.95	1.01
Nb	bdl	bdl	bdl	bdl	bdl	0.0115	0.0104	0.019	0.007	bdl	bdl
La	bdl	bdl	bdl	bdl	bdl	bdl	bdl	bdl	bdl	bdl	bdl
Ce	bdl	bdl	bdl	bdl	bdl	bdl	bdl	0.0055	bdl	bdl	bdl
Pr	bdl	bdl	bdl	0.0056	bdl	0.011	bdl	0.0076	bdl	bdl	bdl
Nd	0.054	0.086	0.266	0.34	0.263	0.189	0.172	0.25	0.111	bdl	bdl
Sm	0.75	1.03	1.65	1.29	1.91	1.58	1.95	2.13	1.75	bdl	0.247
Eu	0.617	0.537	0.562	0.343	0.813	0.378	0.35	0.432	0.339	0.228	0.438
Gd	4.81	2.68	1.88	0.9	4.67	25.6	18.3	18.95	21.32	1.91	3.01
Tb	1.076	0.226	0.146	bdl	0.498	9.09	4.18	4.02	5.6	1.042	0.953
Dy	8.53	1.17	0.77	bdl	2.15	82.1	33.22	28.5	43.7	12.44	8.31
Ho	1.84	0.2	bdl	bdl	0.226	18.55	7.5	5.77	9.88	3.41	2.002
Er	6.4	bdl	bdl	bdl	bdl	61.4	24.53	17.46	30.76	12.6	6.37
Tm	1.03	bdl	bdl	bdl	bdl	8.74	3.4	2.38	4.06	2.02	0.992
Yb	8.1	bdl	bdl	bdl	bdl	61.74	21.64	16.29	24.37	17.74	7.53
Lu	1.6	bdl	bdl	0.088	bdl	9.35	2.93	2.22	3.07	3.16	1.104
Hf	bdl	bdl	bdl	0.035	0.084	0.032	bdl	bdl	0.071	bdl	bdl
Ta	bdl	bdl	bdl	bdl	bdl	0.0128	0.0044	0.023	0.0065	bdl	0.0036
Pb	0.037	bdl	bdl	bdl	bdl	bdl	bdl	bdl	bdl	bdl	bdl
Th	bdl	bdl	bdl	bdl	bdl	bdl	bdl	bdl	bdl	bdl	bdl
U	bdl	bdl	bdl	0.042	bdl	0.03	0.038	0.044	0.031	bdl	bdl

Sample	grt47_39 G12-101	grt47_40 G12-101	grt47_41 G12-101	grt47_42 G12-101	grt47_43 G12-101	grt47_44 G12-101	grt47_45 G12-101	grt47_46 G12-101
Zone	II	III	III	IV	IV	IV	IV	IV
(ppm)								
P	30.4	37.5	40	51.6	57.3	66.1	59.2	75
Ca (wt%)	2.962	4.252	4.455	2.638	1.846	1.589	1.684	1.368
Sc	137.1	111.6	172.1	163.3	158.2	145.9	162	162.7
Ti	155.7	278.7	294	181.8	143	138.8	140.7	150.1
Cr	566	633	880	1603	786.9	710	700	577.2
Mn	23750	11890	6963	6943	1952	2190	2772	3494
Rb	bdl	bdl	bdl	0.249	bdl	bdl	bdl	bdl
Sr	bdl	bdl	bdl	bdl	bdl	bdl	bdl	bdl
Y	76.8	13.34	17.3	70.9	61.2	78.4	79.3	53.79
Zr	0.94	3.52	1.26	1.63	2.78	3.22	3.77	3.85
Nb	bdl	bdl	bdl	bdl	bdl	bdl	bdl	bdl
La	bdl	bdl	bdl	bdl	bdl	bdl	bdl	bdl
Ce	bdl	bdl	bdl	bdl	bdl	bdl	bdl	bdl
Pr	bdl	bdl	bdl	bdl	bdl	0.0071	bdl	bdl
Nd	bdl	bdl	bdl	0.052	0.105	0.205	0.106	0.073
Sm	0.248	bdl	0.13	0.99	1.43	2.52	2.07	1.79
Eu	0.381	0.342	0.464	0.468	0.326	0.314	0.35	0.218
Gd	5.35	1.4	1.51	9.19	6.87	10.5	8.32	7.05
Tb	1.467	0.242	0.342	1.759	1.287	1.75	1.46	1.414
Dy	10.71	2.07	2.42	11.89	9.51	12.25	12.62	8.34
Ho	2.57	0.436	0.539	2.3	2	2.56	2.61	1.78
Er	8.39	1.22	1.94	6.06	6.03	7.57	8.58	4.26
Tm	1.257	0.173	0.312	0.697	0.658	0.882	1.085	0.476
Yb	8.58	1.28	2.63	3.63	3.99	5.08	6.53	2.45
Lu	1.229	0.178	0.4	0.351	0.367	0.536	0.661	0.185
Hf	0.032	0.064	bdl	bdl	bdl	0.041	0.026	bdl
Ta	bdl	bdl	bdl	bdl	bdl	bdl	bdl	bdl
Pb	0.027	0.023	0.045	0.034	bdl	bdl	bdl	bdl
Th	bdl	bdl	bdl	bdl	bdl	bdl	bdl	bdl
U	0.0092	bdl	bdl	bdl	0.02	bdl	bdl	bdl

Spot	zone	$^{18}O/^{16}O$	±SE	meas. $\delta^{18}O$ (‰)	±SE	Xgrs	Xpyr	Xspess	Xalm	BIAS grs	BIAS spess	corr. $\delta^{18}O$ (‰)	±SE
g12-113-6b	I	0.00203830	1.85E-07	8.95	0.09	0.05	0.05	0.09	0.81	-0.76	0.51	**8.91**	**0.28**
g12-113-19	I	0.00203848	2.09E-07	9.04	0.10	0.06	0.05	0.10	0.80	-0.70	0.57	**9.00**	**0.28**
g12-113-44	I	0.00204687	1.01E-07	9.32	0.02	0.06	0.05	0.12	0.77	-0.69	0.70	**9.27**	**0.26**
g12-113-20	I	0.00203895	1.90E-07	9.27	0.09	0.06	0.05	0.12	0.77	-0.66	0.72	**9.23**	**0.27**
g12-113-21	I	0.00203899	2.25E-07	9.30	0.11	0.06	0.04	0.13	0.76	-0.64	0.77	**9.26**	**0.28**
g12-113-7b	I	0.00203919	5.40E-08	9.40	0.03	0.06	0.04	0.14	0.76	-0.69	0.80	**9.35**	**0.26**
g12-113-45x	I	0.00204693	1.25E-07	9.48	0.09	0.07	0.04	0.14	0.75	-0.63	0.85	**9.43**	**0.27**
g12-113-7.5	I	0.00203921	2.02E-07	9.40	0.10	0.06	0.04	0.15	0.75	-0.65	0.87	**9.36**	**0.27**
g12-113-22	I	0.00203896	1.13E-07	9.28	0.06	0.06	0.04	0.16	0.73	-0.64	0.96	**9.24**	**0.26**
g12-113-8b	I	0.00203978	2.06E-07	9.69	0.10	0.06	0.04	0.18	0.72	-0.69	1.04	**9.64**	**0.27**
									Average:			**9.27**	
									Stdev:			**0.21**	
g12-113-5.5	II	0.00203985	1.19E-07	9.72	0.06	0.11	0.04	0.06	0.79	-0.16	0.31	**9.67**	**0.26**
g12-113-26	II	0.00203881	9.10E-08	9.21	0.04	0.09	0.05	0.06	0.81	-0.42	0.33	**9.16**	**0.26**
g12-113-17	II	0.00203853	4.80E-08	9.07	0.02	0.08	0.05	0.06	0.81	-0.43	0.34	**9.03**	**0.26**
g12-113-43	II	0.00204707	1.55E-07	9.42	0.11	0.08	0.05	0.07	0.81	-0.45	0.37	**9.37**	**0.28**
g12-113-18	II	0.00203911	2.04E-07	9.36	0.10	0.08	0.05	0.08	0.79	-0.43	0.45	**9.31**	**0.28**
									Average:			**9.31**	
									Stdev:			**0.24**	
g12-113-23	III	0.00203800	1.50E-07	8.81	0.07	0.10	0.06	0.02	0.83	-0.32	0.06	**8.76**	**0.28**
g12-113-38	III	0.00204642	2.65E-07	9.05	0.14	0.07	0.06	0.02	0.85	-0.57	0.06	**9.01**	**0.30**
g12-113-24	III	0.00203903	1.22E-07	9.31	0.06	0.12	0.05	0.03	0.80	-0.10	0.12	**9.27**	**0.26**
g12-113-3b	III	0.00203962	1.58E-07	9.60	0.08	0.11	0.05	0.01	0.83	-0.16	0.01	**9.56**	**0.28**
g12-113-28	III	0.00203985	5.80E-08	9.72	0.03	0.11	0.05	0.01	0.83	-0.20	0.02	**9.68**	**0.27**
g12-113-39	III	0.00204682	1.47E-07	9.11	0.04	0.07	0.06	0.02	0.85	-0.54	0.04	**9.07**	**0.27**
g12-113-42	III	0.00204667	1.92E-07	9.23	0.07	0.07	0.06	0.02	0.85	-0.59	0.05	**9.19**	**0.28**
g12-113-4b	III	0.00204028	7.80E-08	9.93	0.04	0.10	0.05	0.02	0.82	-0.24	0.07	**9.89**	**0.27**
g12-113-35	III	0.00204806	1.70E-07	9.97	0.15	0.13	0.05	0.02	0.79	0.04	0.09	**9.92**	**0.29**
g12-113-15	III	0.00204005	7.30E-08	9.81	0.04	0.10	0.05	0.03	0.82	-0.31	0.12	**9.77**	**0.27**
g12-113-36	III	0.00204803	1.52E-07	10.18	0.04	0.16	0.04	0.03	0.77	0.27	0.14	**10.13**	**0.27**
g12-113-29	III	0.00204071	1.58E-07	10.14	0.08	0.16	0.04	0.03	0.76	0.31	0.14	**10.09**	**0.27**
g12-113-5b	III	0.00204086	9.60E-08	10.22	0.05	0.14	0.04	0.04	0.78	0.10	0.17	**10.17**	**0.26**
g12-113-25	III	0.00204029	2.44E-07	9.94	0.12	0.14	0.04	0.04	0.78	0.08	0.20	**9.89**	**0.28**
g12-113-37	III	0.00204754	1.23E-07	9.76	0.06	0.13	0.04	0.04	0.79	0.00	0.21	**9.71**	**0.25**
g12-113-16	III	0.00204006	2.02E-07	9.82	0.10	0.14	0.04	0.05	0.77	0.07	0.24	**9.77**	**0.27**
									Average:			**9.62**	
									Stdev:			**0.43**	
g12-113-10	IV	0.00203603	2.00E-07	7.84	0.10	0.03	0.10	0.00	0.87	-0.99	-0.08	**7.80**	**0.29**
g12-113-11	IV	0.00203637	6.50E-08	8.01	0.03	0.05	0.09	0.00	0.87	-0.82	-0.08	**7.97**	**0.27**
g12-113-12	IV	0.00203639	6.80E-08	8.02	0.03	0.06	0.06	0.00	0.88	-0.74	-0.07	**7.98**	**0.27**
g12-113-32	IV	0.00204446	1.85E-07	7.95	0.04	0.06	0.07	0.00	0.87	-0.73	-0.06	**7.91**	**0.27**

Spot	zone	$^{18}O/^{16}O$	±SE	meas. $\delta^{18}O$ (‰)	±SE	Xgrs	Xpyr	Xspess	Xalm	BIAS grs	BIAS spess	corr. $\delta^{18}O$ (‰)	±SE
g12-113-31	IV	0.00204497	1.38E-07	8.15	0.13	0.05	0.07	0.00	0.87	-0.76	-0.06	**8.11**	**0.30**
g12-113-33	IV	0.00204463	1.59E-07	8.04	0.04	0.07	0.07	0.00	0.86	-0.61	-0.05	**8.00**	**0.27**
g12-113-27	IV	0.00203607	1.28E-07	7.86	0.06	0.07	0.06	0.01	0.86	-0.61	-0.03	**7.82**	**0.28**
g12-113-2b	IV	0.00203659	2.43E-07	8.11	0.12	0.05	0.07	0.01	0.87	-0.84	-0.02	**8.07**	**0.30**
g12-113-41	IV	0.00204493	1.88E-07	8.13	0.09	0.06	0.06	0.01	0.86	-0.64	-0.02	**8.09**	**0.29**
g12-113-13	IV	0.00203655	1.99E-07	8.10	0.10	0.06	0.07	0.01	0.86	-0.65	0.00	**8.05**	**0.29**
g12-113-14	IV	0.00203662	1.68E-07	8.13	0.08	0.07	0.06	0.01	0.86	-0.63	0.00	**8.09**	**0.28**
g12-113-30	IV	0.00204445	1.39E-07	7.90	0.05	0.04	0.07	0.01	0.88	-0.90	0.00	**7.86**	**0.28**
g12-113-34	IV	0.00204390	1.96E-07	7.67	0.11	0.08	0.06	0.01	0.85	-0.48	0.00	**7.63**	**0.29**
g12-113-40	IV	0.00204393	1.60E-07	7.85	0.05	0.08	0.06	0.01	0.85	-0.47	0.01	**7.80**	**0.27**
g12-113-1b	outer	0.00203653	1.48E-07	8.08	0.07	0.03	0.10	0.01	0.86	-1.02	-0.03	**8.04**	**0.28**
									Average:			**7.95**	
									Stdev:			**0.14**	

Instrument:	SHRIMP SI
Session:	29/07/13
UWG repeatability:	0.27

Spot	zone	$^{18}O/^{16}O$	±SE	meas. $\delta^{18}O$ (‰)	±SE	Xgrs	Xpyr	Xspess	Xalm	BIAS grs	BIAS spess	corr. $\delta^{18}O$ (‰)	±SE
g12-101-3b	I	0.00203998	2.00E-07	9.78	0.10	0.08	0.05	0.13	0.73	-0.44159	0.769805	**9.74**	**0.27**
g12-101-21	I	0.00204060	6.30E-08	10.09	0.03	0.09	0.04	0.14	0.73	-0.39726	0.821525	**10.04**	**0.25**
g12-101-19	I	0.00203955	1.20E-07	9.57	0.06	0.08	0.05	0.16	0.71	-0.46109	0.922336	**9.53**	**0.26**
g12-101-20	I	0.00203951	7.50E-08	9.55	0.04	0.08	0.05	0.17	0.69	-0.44109	1.002212	**9.51**	**0.25**
g12-101-2b	I	0.00204021	2.08E-07	9.90	0.10	0.08	0.05	0.17	0.70	-0.48183	1.009067	**9.85**	**0.27**
g12-101-22	I	0.00204019	1.86E-07	9.88	0.09	0.08	0.05	0.18	0.70	-0.50623	1.039885	**9.84**	**0.27**
g12-101-23	I	0.00204783	1.06E-07	10.00	0.13	0.08	0.05	0.19	0.69	-0.50231	1.08796	**9.95**	**0.28**
g12-101-1b	I	0.00204084	1.29E-07	10.21	0.06	0.08	0.05	0.19	0.68	-0.48614	1.12007	**10.16**	**0.26**
									Average:			**9.83**	
									Stdev:			**0.23**	
g12-101-16	II	0.00204055	1.00E-08	10.06	0.00	0.15	0.05	0.08	0.72	0.16344	0.465362	**10.01**	**0.25**
g12-101-6b	II	0.00204146	2.53E-07	10.51	0.12	0.21	0.04	0.08	0.67	0.6865	0.465939	**10.46**	**0.29**
g12-101-5b	II	0.00204135	1.99E-07	10.46	0.10	0.15	0.05	0.10	0.70	0.22167	0.56675	**10.41**	**0.27**
g12-101-17	II	0.00204128	1.66E-07	10.42	0.08	0.17	0.04	0.11	0.68	0.37394	0.676908	**10.37**	**0.27**
g12-101-18	II	0.00204123	1.25E-07	10.40	0.06	0.19	0.04	0.14	0.64	0.52358	0.798614	**10.34**	**0.26**
g12-101-4b	II	0.00204156	2.00E-07	10.56	0.10	0.18	0.04	0.14	0.65	0.41034	0.813136	**10.51**	**0.27**
									Average:			**9.42**	
									Stdev:			**2.47**	
g12-101-8b	III	0.00204162	7.20E-08	10.59	0.04	0.22	0.05	0.01	0.72	0.78715	-0.00294	**10.54**	**0.27**
g12-101-14	III	0.00204138	2.28E-07	10.47	0.11	0.20	0.06	0.02	0.73	0.58473	0.056517	**10.42**	**0.29**
g12-101-13	III	0.00203920	3.07E-07	9.40	0.15	0.11	0.07	0.02	0.80	-0.16004	0.056816	**9.35**	**0.30**
g12-101-9b	III	0.00203921	1.05E-07	9.40	0.05	0.12	0.06	0.04	0.79	-0.08437	0.167674	**9.36**	**0.26**
g12-101-7b	III	0.00204147	6.90E-08	10.52	0.03	0.21	0.04	0.04	0.71	0.69393	0.191461	**10.46**	**0.27**
g12-101-15	III	0.00204120	2.68E-07	10.38	0.13	0.19	0.05	0.05	0.71	0.56712	0.255968	**10.33**	**0.29**
									Average:			**10.08**	
									Stdev:			**0.56**	
g12-101-25	IV	0.00204585	1.48E-07	8.76	0.13	0.07	0.09	0.00	0.84	-0.58452	-0.08	**8.72**	**0.30**
g12-101-27	IV	0.00204460	1.42E-07	8.24	0.14	0.05	0.09	0.00	0.85	-0.74334	-0.06993	**8.20**	**0.31**
g12-101-12	IV	0.00203863	2.07E-07	9.12	0.10	0.08	0.09	0.00	0.82	-0.48984	-0.06308	**9.08**	**0.29**
g12-101-24	IV	0.00204553	1.95E-07	8.54	0.04	0.05	0.10	0.00	0.85	-0.78516	-0.05979	**8.50**	**0.27**
g12-101-11b	IV	0.00203805	8.00E-08	8.83	0.04	0.07	0.09	0.01	0.84	-0.59758	-0.04217	**8.79**	**0.27**
g12-101-26	IV	0.00204666	1.71E-07	9.10	0.06	0.09	0.09	0.01	0.82	-0.38763	-0.02746	**9.05**	**0.28**
g12-101-30	IV	0.00204558	1.54E-07	8.63	0.08	0.10	0.07	0.01	0.82	-0.29376	-0.0223	**8.58**	**0.28**
g12-101-10b	IV	0.00203775	2.56E-07	8.68	0.13	0.08	0.08	0.01	0.83	-0.46783	-0.01193	**8.64**	**0.30**
g12-101-29	IV	0.00204632	1.23E-07	8.67	0.06	0.06	0.07	0.02	0.85	-0.70516	0.068045	**8.63**	**0.28**
g12-101-28	IV	0.00204546	1.46E-07	8.33	0.11	0.06	0.07	0.03	0.84	-0.73263	0.146517	**8.29**	**0.29**
									Average:			**8.65**	
									Stdev:			**0.29**	

Instrument:	SHRIMP SI
Session:	29/07/13
UWG repeatability:	0.27

Table Suppl-8a

G12-101	**T = 550°C**		**G12-113**	**T = 610°C**	
mineral	mode	$\delta^{18}O$ (‰)	mineral	mode	$\delta^{18}O$ (‰)
quartz	**6**	13.8	quartz	**43**	13.7
muscovite	**12**	11	muscovite	**11**	11.1
garnet	**15**	**9.4**	garnet	**30**	**9.7**
chlorite	**26**	10.4	chlorite	**7**	10.5
albite	**41**	12.5	staurolite	**9**	11.1
WR		11.4	WR		11.7

Mineral modes were estimated for samples G12-101 and G-12-113 using thin section observations and adjusted using WR XRF data for K_2O, NaO and CaO to constrain modes of white mica and plagioclase; the same minerals and modes were used for the three garnet zones: the estimate of quartz in the assemblage is most critical for oxygen isotope fractionation as quartz has the highest $\delta^{18}O$. The fractionation factors used are from Zheng (1993a, 1993b).

Table Suppl-8b

Analysis type	T (°C)	G12-101		G12-113	
		Measured gt	Modelled WR	Measured gt	Modelled WR
Garnet core (I)	550	9.4 ± 0.2	11.4	9.2 ± 0.1	11.5
Garnet II	610	9.4 ± 0.2	11.2	9.7 ± 0.3	11.7
Garnet III	610	9.7 ± 0.1	11.5	9.4 ± 0.2	11.4
Garnet rim (IV)	500	9.3 ± 0.2	11.5	8.7 ± 0.3	11.2
Measured WR			**11.6**		**11.5**